A Detailed Chemical Kinetic Model for High Temperature Ethanol Oxidation

NICK M. MARINOV

Lawrence Livermore National Laboratory, P.O. Box 808, *Livermore*, CA 94550

Received 20 August 1998; accepted 15 October 1998

ABSTRACT: A detailed chemical kinetic model for ethanol oxidation has been developed and validated against a variety of experimental data sets. Laminar flame speed data (obtained from a constant volume bomb and counterflow twin-flame), ignition delay data behind a reflected shock wave, and ethanol oxidation product profiles from a jet-stirred and turbulent flow reactor were used in this computational study. Good agreement was found in modeling of the data sets obtained from the five different experimental systems. The computational results show that high temperature ethanol oxidation exhibits strong sensitivity to the fall-off kinetics of ethanol decomposition, branching ratio selection for $C_2H_5OH + OH \leftrightarrow$ Products, and reactions involving the hydroperoxyl (HO_2) radical.

The multichanneled ethanol decomposition process is analyzed by RRKM/Master Equation theory, and the results are compared with those obtained from earlier studies. The ten-parameter Troe form is used to define the $C_2H_5OH(+M) \leftrightarrow CH_3 + CH_2OH(+M)$ rate expression as

$$k^{\infty} = 5.94E23\ T^{-1.68} \exp(-45880\ K/T)\ (s^{-1})$$
$$k^{o} = 2.88E85\ T^{-18.9} \exp(-55317\ K/T)\ (cm^3/mol/sec)$$
$$F_{cent} = 0.5 \exp(-T/200\ K) + 0.5 \exp(-T/890\ K) + \exp(-4600\ K/T)$$

and the $C_2H_5OH(+M) \leftrightarrow C_2H_4 + H_2O(+M)$ rate expression as

$$k^{\infty} = 2.79E13\ T^{0.09} \exp(-33284\ K/T)\ (s^{-1})$$
$$k^{o} = 2.57E83\ T^{-18.85} \exp(-43509\ K/T)\ (cm^3/mol/sec)$$
$$F_{cent} = 0.3 \exp(-T/350\ K) + 0.7 \exp(-T/800\ K) + \exp(-3800\ K/T)$$

with an applied energy transfer per collision value of $\langle \Delta E_{down} \rangle = 500\ cm^{-1}$.

An empirical branching ratio estimation procedure is presented which determines the temperature dependent branching ratios of the three distinct sites of hydrogen abstraction from ethanol. The calculated branching ratios for $C_2H_5OH + OH$, $C_2H_5OH + O$, $C_2H_5OH + H$, and $C_2H_5OH + CH_3$ are compared to experimental data. © 1999 John Wiley & Sons, Inc.* Int J Chem Kinet 31: 183–220, 1999

Correspondence to: N. M. Marinov

Contract grant Sponsor: U.S. Department of Energy/Lawrence Livermore Natl. Lab.

Contract grant number: W-7405-ENG-48

 CCC 0538-8066/99/030183-38

INTRODUCTION

In recent years, considerable interest in ethanol as a fuel extender, octane enhancer, oxygenate, and a neat

fuel has increased dramatically because of concerns associated with conventional transportation fuels. The elimination of tetra-ethyl lead in gasoline during the mid-1980s and the 1990 Clean Air Act Amendments have required refinery operations to provide oxygenated gasoline in order to meet octane quality demands and reduce carbon monoxide emissions and smog in the nation's most polluted areas. Currently, ethanol and methyl tert-butyl ether (MTBE) are the most widely used oxygenated fuels, and are most commonly used in Federal and California reformulated gasoline and winter oxygenated gasoline in the Western United States. Ethanol may be considered as the preferred oxygenate since MTBE is a suspected carcinogen. Furthermore, ethanol possesses the advantage of being produced from renewable fuels like biomass while MTBE requires isobutene, a waste fossil fuel product in the gasoline refining process, for synthesis, and ethanol has roughly double the oxygen content than MTBE on an oxygen to carbon basis. Recently, MTBE has been reported as a drinking water contaminant in urban wells, aquifers, springs, and municipal water reservoirs across the United States, especially in California [1]. The potential removal of MTBE from reformulated gasoline has greatly renewed interest in ethanol as a gasoline additive.

There are fundamental and practical reasons for examining the oxidation of ethanol. Approximately 6–10 vol % of reformulated gasoline may consist of ethanol, as required by current federal and state urban air quality standards. As regulations on pollutant emissions become stricter, the amount of oxygenated fuel like ethanol in gasoline could increase. Therefore, we need a full understanding of the reaciton pathways by which ethanol is oxidized and of the pollutant species that it may produce. This understanding will allow industry and regulatory agencies to better evaluate the feasibility and relationship between the combustion process and pollutant emissions when using ethanol.

Previous detailed chemical kinetic modeling studies performed during the early 1990s have greatly improved the level of understanding of the ethanol oxidation and pyrolysis process since the original modeling work of Natarajan and Bhaskaran [2]. These modeling efforts focused on problems of ethanol ignition delay from shock tubes [2,3,4,7], ethanol laminar flame speeds in burners [4,7], and product profiles from ethanol pyrolysis and oxidation studies in static [5], turbulent flow [4,6], and jet-stirred reactors [7]. Additional evidence of mechanistic features important to describing ethanol reaction kinetics from static [8–11] and flow reactors [12–14], and information on autoignition characteristics in a rapid compression machine [15] and combustion bomb [16], pressure, temperature, and mixture strength effects on flame propagation rates [17] or modes of formation of soot in diffusion flames [18,19] have proven to be useful for ethanol model development. These experimental works have been previously summarized [6] and no further elaboration will be presented. The important issues raised in the previous modeling works concern specific features of the ethanol reaction kinetics, in particular, the branching ratio assignments for the H-atom abstraction reactions from ethanol and the fall-off kinetics of the ethanol decomposition reactions.

The modeling studies of Borisov et al. [5] and Norton and Dryer [6] were the first to address the issue of the three distinct H-atom sites in ethanol and the resulting temperature dependent product distribution during its combustion. Their modeling studies showed good agreement with the time history of the reaction products evolution during ethanol pyrolysis and oxidation. These results emphasized the importance of distinguishing the three C_2H_5O isomers that form through H-atom abstraction from ethanol, and the branching ratio assignments for proper product determination. However, these authors also noted that the narrow temperature range of their experiments prevented the determination of the branching ratio dependence with temperature. These authors agree that additional work is needed to clarify the nature of the temperature dependent behavior of the branching ratios for $C_2H_5OH + X \leftrightarrow \{CH_2CH_2OH, CH_3CHOH, CH_3CH_2O\} + XH$ $\{X = OH, O, H, CH_3, HO_2, \text{etc.}\}$.

The shock tube modeling work for ethanol has shown contradictory findings, especially concerning the nature of the pressure dependence involving the $C_2H_5OH(+M) \leftrightarrow CH_3 + CH_2OH(+M)$ decomposition reaction and those reactions that exhibit the greatest sensitivity to ignition delay. The important chain initiation step for shock tube conditions, $C_2H_5OH(+M) \leftrightarrow CH_3 + CH_2O(+M)$, has been previously assumed to exhibit second-order behavior in the reflected shock ignition delay modeling study of Natarajan and Bhaskaran [2], and Dunphy and Simmie [3], or the reaction was shown to be in the fall-off, psuedo-first order region by Borisov et al. in reflected shock pyrolysis experiments. These studies were conducted at very similar conditions of pressure and temperature. Further complications were shown in the modeling and sensitivity analysis study of ethanol ignition delays by Dunphy and Simmie [3], Curran et al. [3,20], Egolfopoulos et al. [4], and Dagaut et al. [7]. Egolfopoulos demonstrated good modeling agreement with the Natarajan ignition delay data sets for equivalence ratios of 0.5–2.0, and found $C_2H_5OH \leftrightarrow CH_3 + CH_2OH$ as the most sensitive reaction to ignition delay which agreed with the earlier finding of Natarajan.

However, Curran, Dagaut, and Dunphy found a lack of sensitivity for this chain initating ethanol decomposition reaction when modeling ignition delays from reflected shocks of various $C_2H_5OH—O_2—Ar$ mixture strengths at conditions of 1100–1900 K and 2.0–4.5 bar. Curran showed the ethanol ignition delay to be most sensitive to $H + O_2 \leftrightarrow O + OH$, $H + O_2 + M \leftrightarrow HO_2 + M$, $CH_3 + HO_2 \leftrightarrow CH_3O + OH$, and $H_2 + OH \leftrightarrow H_2O + H$ reactions. These sensitivity analysis results were similar to the sensitivity analysis findings of Dunphy and Dagaut. Also, the Curran modeling efforts suggested that ethanol decomposition occurs at or very near the high pressure limit for the conditions of their study [20]. This particular result differs from the earlier findings of Borisov et al. and the assumption made by Natarajan and Dunphy.

The primary objective of the current study is to present new rate constant expressions for ethanol decomposition and H-atom abstraction reactions from ethanol, as well as to develop and validate a detailed chemical kinetic model for ethanol oxidation by comparison with experimental data sets obtained under a variety of high temperature conditions. The modeling study examined ignition delay data from shock tubes, laminar flame speed data from a combustion bomb and a counterflow twin flame, and species profiles from ethanol oxidation in jet-stirred and turbulent flow reactors. The data sets considered span the temperature range of 1000–1700 K, a pressure range of 1.0–4.5 atm, and an equivalence ratio range of 0.5–2.0. This objective is to be achieved by an empirical branching ratio estimation procedure that determines the temperature dependent branching ratios of the three distinct sites of hydrogen abstraction from ethanol, fall-off rate constant calculations for the multichanneled ethanol decomposition process, and reaction pathway and sensitivity analysis. The latter approach is extensively used in order to help in the model refinement and to identify those reactions and their accompanying rate constants that exhibit a strong influence on the ethanol oxidation process. Hopefully, the results of this work will lead to an improved level of understanding of the high temperature ethanol oxidation process.

DISCUSSION OF THE COMPUTATIONAL MODELS

The modeling computations were performed using the CHEMKIN-II software [21] in conjunction with the SENKIN [22], PREMIX [23], and PSR [24] programs. The SENKIN program predicts the time-dependent chemical kinetics behavior of a homogeneous gas phase mixture in a closed system. This particular program was used to calculate ignition delays in a shock tube, and to study fuel oxidation in a turbulent flow reactor. The ignition delay calculations were performed by assuming an adiabatic system and a constant density gas behind the reflected shock wave. The flow reactor calculations were performed at constant pressure with the additional constraint of using the experimentally measured temperature profile as suggested by Norton and Dryer [6]. The laminar flame speed calculations were performed using the PREMIX code for freely propagating flames. These computations require the flame front to be one-dimensional with no heat loss to the surroundings. The central differencing technique was used in the numerical integration of the laminar flame speeds at unburned gas conditions of 1.0 atm and 298 K. The upwind differencing scheme was used for calculations performed at pressures greater than 1.0 atm and unburned gas temperatures greater than 450 K. Two hundred zones and greater were used in the upwind differencing integrations. Thermal diffusion was included in the adiabatic freely propagating flame calculations. The PSR (perfectly-stirred reactor) program was used to calculate the species concentrations for the jet-stirred reactor study. The PSR code determines the steady-state species composition in the reactor per prescribed temperature. The PSR simulation requires the important assumption that the rate of conversion from reactants to products is controlled by the chemical reaction rates and not by the mixing process. This assumption requires the mixing process to be infinitely fast, and as a consequence no spatial temperature and concentration gradients are found in the stirred reactor.

The detailed chemical kinetic model was assembled using reaction submechanisms developed previously for hydrogen [25], methane [26], ethylene [27,28], ethane [26], and propane oxidation [29]. The hierarchical nature of the model development for the C_3 hydrocarbon submechanism relied on using literature-based kinetic data whenever possible, evaluated kinetic rate constant information, theoretically calculated rate parameters, and rate constant estimations based on analogies to similar reactions. The compiled ethanol oxidation mechanism is listed in Table I and consists of 56 species and 351 reversible reactions. Third body efficiencies and pressure corrections were applied as necessary to the dissociation, recombination, and addition reactions. These reactions are expressed in either the ten parameter Troe format or in the Lindemann-Hinshelwood description for fall-off kinetics.

Transport properties were obtained from the Sandia CHEMKIN transport data base [30] as found in the TRANDAT file of the Sandia TRANFIT program.

Transport properties for species not found in the database were estimated using the methods described by Wang and Frenklach [31].

The thermodynamic properties for the species used in this study were primarily obtained from the CHEMKIN thermodynamic database [32], and Burcat and McBride [33]. Thermodynamic properties for those species not found in the databases were estimated by group additivity [34–36]. These estimated specific heats, standard state enthalpies, and standard state entropies data were fitted for the 300–1500 K range and extrapolated to 5000 K using the Harmonic Oscillator Equation and Exponential Function methods of THERM [36]. The THERM program generates the fourteen polynomial coefficients as used in the NASA Complex Equilibrium program [37]. The compiliation of the thermochemical data in polynomial coefficient along with the reaction kinetics and transport may be obtained by e-mail from the author (marinov1@llnl.gov). Table II shows the thermodynamic data used in this study that is not presently found in the Sandia CHEMKIN Thermodynamic database report [32].

DISCUSSION OF THE REACTION KINETICS

Branching Ratios for H-Atom Abstraction Reactions from Ethanol

The ethanol submechanism was developed by thoroughly reviewing the kinetics literature for rate constants and branching ratios of elementary reactions involving C_2H_5OH, CH_3CHOH, C_2H_4OH, CH_3CH_2O, and CH_3HCO. The detailed chemical kinetic model treats all three distinct sites of hydrogen abstraction in the ethanol molecule, and therefore the model considers the subsequent reactions of all three isomers of C_2H_5O (i.e., CH_3CHOH, C_2H_4OH, and CH_3CH_2O). Currently, a very limited amount of direct branching ratio information exists for H-atom abstraction reactions involving ethanol. Direct measurements of branching ratios can be found for temperatures below 600 K, and at 3500 K for $C_2H_5OH + OH$ [38,39], $C_2H_5OH + O$ [40,41], and $C_2H_5OH + CH_3$ [42] reactions. However, these data may not be applicable to the conditions examined in the present study. Previous modeling efforts have treated the branching ratios by either (1) using a total overall rate constant for $C_2H_5OH + X$ (where, X = OH,O,H, and CH_3) and partitioning the overall rate constant by temperature independent branching ratios for the various abstractable H-atom sites [6], or (2) using rate constants from analogous reactions that exhibit similar bond strengths as found in ethanol without constraining the overall rate constant [20]. The success of the first approach is dependent on having a complete understanding of the combustion chemistry of ethanol and its reaction intermediates. The second approach fails to enforce the overall $C_2H_5OH + X \leftrightarrow$ Products rate constant, and assumes the correct temperature dependent branching ratios would fall out from the analogous abstraction rate constants in $C_3H_8 + X$ and $CH_3OH + X$ as assigned to $C_2H_5OH + X$. In this study, it is expected that the branching ratios will exhibit temperature dependence, and that a simple methodology would have to be adopted in order to extrapolate the measured low temperature branching ratios to high temperature conditions or to make predictions in absence of direct branching ratio measurements. The following approach was adopted which uses previously determined branching ratio values from model compounds that exhibit similar structural and chemical bonding characteristics as those found in ethanol. Propane and methanol were used as the model compounds to treat the relative branching ratios for the three specific H-atom abstraction sites in ethanol. This was done as ample experimental and theoretical information exists at elevated temperatures on the relative rates of H-atom abstraction from these species.

Propane and methanol have very similar O—H and C—H bond strengths as found in ethanol. This is shown in Figure 1. The similarity in bond strengths and structural characteristics between the model compounds and ethanol allows for a set of equations to be developed and solved. The relative rates of H-atom abstrac-

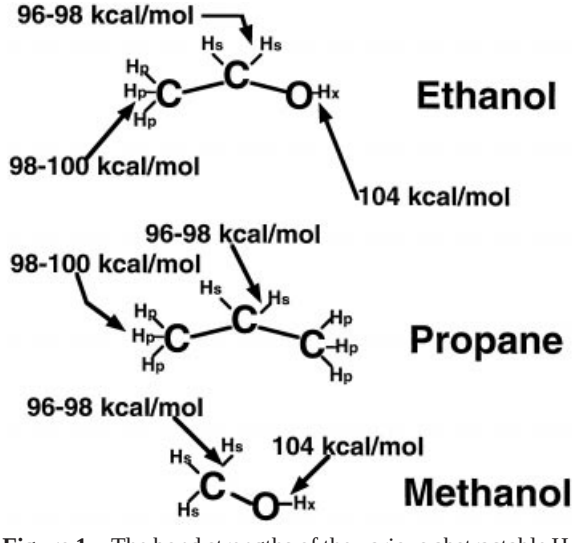

Figure 1 The bond strengths of the various abstractable H-atoms from ethanol, propane, and methanol.

Table I Reaction Mechanism Rate Coefficients ($k_f = A\,T^b \exp(-E_a/RT)$, Units are Moles, cm^3, Seconds, K, and Calories/Mole)

Reaction	A	b	E_a	Reference
HYDROGEN–OXYGEN SUBMECHANISM				
1. $OH + H_2 = H + H_2O$	2.14E + 08	1.52	3449.0	[25]
2. $O + OH = O_2 + H$	2.02E + 14	−0.4	0.0	[25]
3. $O + H_2 = OH + H$	5.06E + 04	2.67	6290.0	[25]
4. $H + O_2(+M) = HO_2(+M)^\alpha$	4.52E + 13	0.0	0.0	[25]
Low pressure limit:	1.05E + 19	−1.257	0.0	
Enhanced Third Body Efficiencies:				
$H_2O = 0.0$, $H_2 = 0.0$, $N_2 = 0.0$, $CH_4 = 10.0$,				
$CO_2 = 3.8$, $CO = 1.9$				
4a. $H + O_2(+N_2) = HO_2(+N_2)$	4.52E + 13	0.0	0.0	[25]
Low pressure limit:	2.03E + 20	−1.59	0.0	
4b. $H + O_2(+H_2) = HO_2(+H_2)$	4.52E + 13	0.0	0.0	[25]
Low pressure limit:	1.52E + 19	−1.133	0.0	
4c. $H + O_2(+H_2O) = HO_2(+H_2O)$	4.52E + 13	0.0	0.0	[25]
Low pressure limit:	2.10E + 23	−2.437	0.0	
5. $OH + HO_2 = H_2O + O_2$	2.13E + 28	−4.827	3500.0	[26]
Duplicate reaction				
$OH + HO_2 = H_2O + O_2$	9.10E + 14	0.0	10964.	
Duplicate reaction				
6. $H + HO_2 = OH + OH$	1.50E + 14	0.0	1000.0	[25]
7. $H + HO_2 = H_2 + O_2$	6.63E + 13	0.0	2126.0	[65]
8. $H + HO_2 = O + H_2O$	3.01E + 13	0.0	1721.0	[25]
9. $O + HO_2 = O_2 + OH$	3.25E + 13	0.0	0.0	[25]
10. $2OH = O + H_2O$	3.57E + 04	2.4	−2112.0	[25]
11. $H + H + M = H_2 + M$	1.00E + 18	−1.0	0.0	[25]
Enhanced Third Body Efficiencies:				
$H_2O = 0.0$, $H_2 = 0.0$				
11a. $H + H + H_2 = H_2 + H_2$	9.20E + 16	−0.6	0.0	[25]
11b. $H + H + H_2O = H_2 + H_2O$	6.00E + 19	−1.25	0.0	[25]
12. $H + OH + M = H_2O + M$	2.21E + 22	−2.0	0.0	[25]
Enhanced Third Body Efficiencies:				
$H_2O = 6.4$				
13. $H + O + M = OH + M$	4.71E + 18	−1.0	0.0	[25]
$H_2O = 6.4$				
14. $O + O + M = O_2 + M$	1.89E + 13	0.0	−1788.0	[25]
15. $HO_2 + HO_2 = H_2O_2 + O_2$	4.20E + 14	0.0	11982.0	[25]
Duplicate reaction				
$HO_2 + HO_2 = H_2O_2 + O_2$	1.30E + 11	0.0	−1629.0	
Duplicate reaction				
16. $OH + OH(+M) = H_2O_2(+M)^\beta$	1.24E + 14	−0.37	0.0	[25]
Low pressure limit:	3.04E + 30	−4.63	2049.0	[25]
Troe Parameters: $a = 0.470$, $T^{***} = 100.0$,				
$T^* = 2000.0$				
$T^{**} = 1.0E + 15$				
17. $H_2O_2 + H = HO_2 + H_2$	1.98E + 06	2.0	2435.0	[25]
18. $H_2O_2 + H = OH + H_2O$	3.07E + 13	0.0	4217.0	[25]
19. $H_2O_2 + O = OH + HO_2$	9.55E + 06	2.0	3970.0	[25]
20. $H_2O_2 + OH = H_2O + HO_2$	2.40E + 00	4.042	−2162.0	[25]
C_1 HYDROCARBON SUBMECHANISM				
21. $CH_3 + CH_3(+M) = C_2H_6(+M)$	9.22E + 16	−1.174	636.0	[26]
Low pressure limit:	1.14E + 36	−5.246	1705.0	[26]
Troe Parameters: $a = 0.405$, $T^{***} = 1120.0$,				
$T^* = 69.6$, $T^{**} = 1.0E + 15$				
Enhanced Third Body Efficiencies:				
$H_2O = 5.0$, $H_2 = 2.0$, $CO_2 = 3.0$, $CO = 2.0$				

(Continued)

Table I (Continued)

Reaction	A	b	E_a	Reference
22. $CH_3 + H(+M) = CH_4(+M)$	2.14E + 15	−0.4	0.0	[26]
Low pressure limit:	3.31E + 30	−4.0	2108.0	
Troe Parameters: $a = 0.0$, $T^{***} = 1.0E - 15$, $T^{*} = 1.0E - 15$, $T^{**} = 40$.				
Enhanced Third Body Efficiencies: $H_2O = 5.0$, $H_2 = 2.0$, $CO_2 = 3.0$, $CO = 2.0$				
23. $CH_4 + H = CH_3 + H_2$	2.20E + 04	3.0	8750.0	[26]
24. $CH_4 + OH = CH_3 + H_2O$	4.19E + 06	2.0	2547.0	[26]
25. $CH_4 + O = CH_3 + OH$	6.92E + 08	1.56	8485.0	[26]
26. $CH_4 + HO_2 = CH_3 + H_2O_2$	1.12E + 13	0.0	24640.0	[26]
27. $CH_3 + HO_2 = CH_3O + OH$	7.00E + 12	0.0	0.0	[26]
28. $CH_3 + HO_2 = CH_4 + O_2$	3.00E + 12	0.0	0.0	[26]
29. $CH_3 + O = CH_2O + H$	8.00E + 13	0.0	0.0	[26]
30. $CH_3 + O_2 = CH_3O + O$	1.45E + 13	0.0	29209.0	[26]
31. $CH_3 + O_2 = CH_2O + OH$	2.51E + 11	0.0	14640.0	[26]
32. $CH_3O + H = CH_3 + OH$	1.00E + 13	0.0	0.0	(a)
33. $CH_2OH + H = CH_3 + OH$	1.00E + 13	0.0	0.0	(a)
34. $CH_3 + OH = CH_2(s) + H_2O$	2.00E + 13	0.0	550.0	[66]
35. $CH_3 + OH = CH_2 + H_2O$	3.00E + 06	2.0	2500.0	[26]
36. $CH_3 + OH = HCOH + H_2$	1.00E + 10	0.0	−415.0	[66]
37. $CH_3 + H = CH_2 + H_2$	9.00E + 13	0.0	15100.0	[26]
38. $CH_3 + M = CH + H_2 + M$	6.90E + 14	0.0	82469.0	[26]
39. $CH_3 + M = CH_2 + H + M$	1.90E + 16	0.0	91411.0	[26]
40. $CH_3 + OH(+M) = CH_3OH(+M)$	8.70E + 13	0.1	0.0	[26]
Low pressure limit:	5.75E + 41	−7.4	626.0	
Troe Parameters: $a = 0.025$, $T^{***} = 1.0E - 15$, $T^{*} = 8000.0$, $T^{**} = 3000.0$				
Enhanced Third Body Efficiencies: $H_2O = 10.0$, $H_2 = 2.0$, $CO_2 = 3.0$, $CO = 2.0$				
41. $CH_3OH(+M) = CH_2(s) + H_2O(+M)$	2.84E + 10	1.00	83871.0	(b,c)
Low pressure limit:	1.78E + 49	−8.81	93369.0	
Troe Parameters: $a = 0.90$, $T^{***} = 740.$, $T^{*} = 980.$, $T^{**} = 5100.$				
Enhanced Third Body Efficiencies: $H_2O = 10.0$, $H_2 = 2.0$, $CO_2 = 3.0$, $CO = 2.0$				
42. $CH_3OH(+M) = HCOH + H_2(+M)$	4.20E + 09	1.12	85604.0	(b,c)
Low pressure limit:	5.02E + 47	−8.40	94823.0	
Troe Parameters: $a = 0.9$, $T^{***} = 615.$, $T^{*} = 915.$, $T^{**} = 4615.$				
Enhanced Third Body Efficiencies: $H_2O = 10.0$, $H_2 = 2.0$, $CO_2 = 3.0$, $CO = 2.0$				
43. $CH_3OH(+M) = CH_2O + H_2(+M)$	2.03E + 09	1.00	91443.0	(b,c)
Low pressure limit:	9.78E + 47	−8.40	101761.0	
Troe Parameters: $a = 0.9$, $T^{***} = 825.$, $T^{*} = 1125.$, $T^{**} = 5700.$				
Enhanced Third Body Efficiencies: $H_2O = 10.0$, $H_2 = 2.0$, $CO_2 = 3.0$, $CO = 2.0$				
44. $CH_3OH + OH = CH_2OH + H_2O$	2.61E + 05	2.182	−1344.0	[26]
45. $CH_3OH + OH = CH_3O + H_2O$	2.62E + 06	2.056	916.0	[26]
46. $CH_3OH + O = CH_2OH + OH$	3.88E + 05	2.5	3080.0	[26]
47. $CH_3OH + H = CH_2OH + H_2$	1.70E + 07	2.1	4868.0	[26]
48. $CH_3OH + H = CH_3O + H_2$	4.24E + 06	2.1	4868.0	[26]
49. $CH_3OH + CH_3 = CH_2OH + CH_4$	3.19E + 01	3.17	7171.0	[26]

(Continued)

Table I (Continued)

Reaction	A	b	E_a	Reference
50. $CH_3OH + CH_3 = CH_3O + CH_4$	1.45E + 01	3.10	6935.0	[26]
51. $CH_3OH + HO_2 = CH_2OH + H_2O_2$	9.64E + 10	0.0	12578.0	[26]
52. $CH_2O + H(+M) = CH_3O(+M)$	5.40E + 11	0.454	2600.0	[67]
Low pressure limit:	1.50E + 30	−4.80	5560.0	
Troe Parameters: $a = 0.758$, $T^{***} = 94.$, $T^{*} = 1555.$, $T^{**} = 4200.$				
Enhanced Third Body Efficiencies: $H_2O = 5.0$				
53. $CH_2O + H(+M) = CH_2OH(+M)$	5.40E + 11	0.454	3600.0	[67]
Low pressure limit:	9.10E + 31	−4.82	6530.0	
Troe Parameters: $a = 0.719$, $T^{***} = 103.$, $T^{*} = 1291.$, $T^{**} = 4160.$				
Enhanced Third Body Efficiencies: $H_2O = 5.0$				
54. $CH_3O + CH_3 = CH_2O + CH_4$	1.20E + 13	0.0	0.0	[67]
55. $CH_3O + H = CH_2O + H_2$	2.00E + 13	0.0	0.0	[26]
56. $CH_2OH + H = CH_2O + H_2$	2.00E + 13	0.0	0.0	[26]
57. $CH_3O + OH = CH_2O + H_2O$	1.00E + 13	0.0	0.0	[26]
58. $CH_2OH + OH = CH_2O + H_2O$	1.00E + 13	0.0	0.0	[26]
59. $CH_3O + O = CH_2O + OH$	1.00E + 13	0.0	0.0	[26]
60. $CH_2OH + O = CH_2O + OH$	1.00E + 13	0.0	0.0	[26]
61. $CH_3O + O_2 = CH_2O + HO_2$	6.30E + 10	0.0	2600.0	[26]
62. $CH_2OH + O_2 = CH_2O + HO_2$	1.57E + 15	−1.0	0.0	[26]
Duplicate reaction				
$CH_2OH + O_2 = CH_2O + HO_2$	7.23E + 13	0.0	3577.0	
Duplicate reaction				
63. $HCOH + OH = HCO + H_2O$	2.00E + 13	0.0	0.0	[26]
64. $HCOH + H = CH_2O + H$	2.00E + 14	0.0	0.0	[26]
65. $HCOH + O = CO + OH + H$	8.00E + 13	0.0	0.0	[26]
66. $HCOH + O_2 = CO + OH + OH$	1.00E + 13	0.0	0.0	[26]
67. $HCOH + O_2 = CO_2 + H_2O$	1.00E + 13	0.0	0.0	[26]
68. $HCOH = CH_2O$	2.10E + 19	−3.07	31700.0	[68](d)
69. $CH_2 + H = CH + H_2$	1.00E + 18	−1.56	0.0	[26]
70. $CH_2 + OH = CH + H_2O$	1.13E + 07	2.0	3000.0	[26]
71. $CH_2 + OH = CH_2O + H$	2.50E + 13	0.0	0.0	[26]
72. $CH_2 + CO_2 = CH_2O + CO$	1.10E + 11	0.0	1000.0	[26]
73. $CH_2 + O = CO + H + H$	5.00E + 13	0.0	0.0	[26]
74. $CH_2 + O = CO + H_2$	3.00E + 13	0.0	0.0	[26]
75. $CH_2 + O_2 = CH_2O + O$	3.29E + 21	−3.3	2868.0	[26]
76. $CH_2 + O_2 = CO_2 + H + H$	3.29E + 21	−3.3	2868.0	[26]
77. $CH_2 + O_2 = CO_2 + H_2$	1.01E + 21	−3.3	1508.0	[26]
78. $CH_2 + O_2 = CO + H_2O$	7.28E + 19	−2.54	1809.0	[26]
79. $CH_2 + O_2 = HCO + OH$	1.29E + 20	−3.3	284.0	[26]
80. $CH_2 + CH_3 = C_2H_4 + H$	4.00E + 13	0.0	0.0	[26]
81. $CH_2 + CH_2 = C_2H_2 + H + H$	4.00E + 13	0.0	0.0	[26]
82. $CH_2 + HCCO = C_2H_3 + CO$	3.00E + 13	0.0	0.0	[26]
83. $CH_2 + C_2H_2 = H_2CCCH + H$	1.20E + 13	0.0	6600.0	[26]
84. $CH_2(s)^{\ddagger} + M = CH_2 + M$	1.00E + 13	0.0	0.0	[26]
Enhanced Third Body Efficiencies: $H = 12.0$, $C_2H_2 = 4.0$, $H_2O = 3.0$				
85. $CH_2(s) + CH_4 = CH_3 + CH_3$	4.00E + 13	0.0	0.0	[26]
86. $CH_2(s) + C_2H_6 = CH_3 + C_2H_5$	1.20E + 14	0.0	0.0	[26]
87. $CH_2(s) + O_2 = CO + OH + H$	7.00E + 13	0.0	0.0	[26]
88. $CH_2(s) + H_2 = CH_3 + H$	7.00E + 13	0.0	0.0	[26]
89. $CH_2(s) + C_2H_2 = H_2CCCH + H$	1.50E + 14	0.0	0.0	[26]

(Continued)

Table I (Continued)

Reaction	A	b	E_a	Reference
90. $CH_2(s) + C_2H_4 = AC_3H_5 + H$	1.30E + 14	0.0	0.0	[26]
91. $CH_2(s) + O = CO + H + H$	3.00E + 13	0.0	0.0	[26]
92. $CH_2(s) + OH = CH_2O + H$	3.00E + 13	0.0	0.0	[26]
93. $CH_2(s) + H = CH + H_2$	3.00E + 13	0.0	0.0	[26]
94. $CH_2(s) + CO_2 = CH_2O + CO$	3.00E + 12	0.0	0.0	[26]
95. $CH_2(s) + CH_3 = C_2H_4 + H$	2.00E + 13	0.0	0.0	[26]
96. $CH_2(s) + CH_2CO = C_2H_4 + CO$	1.60E + 14	0.0	0.0	[26]
97. $CH + O_2 = HCO + O$	3.30E + 13	0.0	0.0	[26]
98. $CH + O = CO + H$	5.70E + 13	0.0	0.0	[26]
99. $CH + OH = HCO + H$	3.00E + 13	0.0	0.0	[26]
100. $CH + CO_2 = HCO + CO$	3.40E + 12	0.0	690.0	[26]
101. $CH + H_2O = CH_2O + H$	1.17E + 15	−0.75	0.0	[26]
102. $CH + CH_2O = CH_2CO + H$	9.46E + 13	0.0	−515.0	[26]
103. $CH + C_2H_2 = C_3H_2 + H$	1.00E + 14	0.0	0.0	[26]
104. $CH + CH_2 = C_2H_2 + H$	4.00E + 13	0.0	0.0	[26]
105. $CH + CH_3 = C_2H_3 + H$	3.00E + 13	0.0	0.0	[26]
106. $CH + CH_4 = C_2H_4 + H$	6.00E + 13	0.0	0.0	[26]
107. $CH_2O + OH = HCO + H_2O$	3.43E + 09	1.18	−447.0	[26]
108. $CH_2O + H = HCO + H_2$	2.19E + 08	1.77	3000.0	[26]
109. $CH_2O + M = HCO + H + M$	3.31E + 16	0.0	81000.0	[26]
110. $CH_2O + O = HCO + OH$	1.80E + 13	0.0	3080.0	[26]
111. $HCO + O_2 = HO_2 + CO$	7.58E + 12	0.0	410.0	[26]
112. $HCO + M = H + CO + M$	1.86E + 17	−1.0	17000.0	[26]
Enhanced Third Body Efficiencies: $H_2O = 5.0$, $H_2 = 1.87$, $CO_2 = 3.0$, CO = 1.87, $CH_4 = 2.81$				
113. $HCO + OH = H_2O + CO$	1.00E + 14	0.0	0.0	[26]
114. $HCO + H = CO + H_2$	1.19E + 13	0.25	0.0	[26]
115. $HCO + O = CO + OH$	3.00E + 13	0.0	0.0	[26]
116. $HCO + O = CO_2 + H$	3.00E + 13	0.0	0.0	[26]
117. $HCOOH + M = CO + H_2O + M$	2.09E + 14	0.0	40400.0	[69]
118. $HCOOH + M = CO_2 + H_2 + M$	1.35E + 15	0.0	60600.0	[69]
119. $HCOOH + OH = CO_2 + H_2O + H$	2.62E + 06	2.056	916.0	(e)
120. $HCOOH + OH = CO + H_2O + OH$	1.85E + 07	1.50	−962.0	(f)
121. $HCOOH + H = CO_2 + H_2 + H$	4.24E + 06	2.10	4868.0	(e)
122. $HCOOH + H = CO + H_2 + OH$	6.06E + 13	−0.35	2988.0	(f)
123. $HCOOH + CH_3 = CH_4 + CO + OH$	3.90E − 07	5.80	2200.0	(f)
124. $HCOOH + HO_2 = CO + H_2O_2 + OH$	2.40E + 19	−2.20	14030.0	(f)
125. $HCOOH + O = CO + OH + OH$	1.77E + 18	−1.90	2975.0	(f)
126. $CO + OH = CO_2 + H$	9.42E + 03	2.25	−2351.0	[26]
127. $CO + O + M = CO_2 + M$	6.17E + 14	0.0	3000.0	[26]
128. $CO + O_2 = CO_2 + O$	2.53E + 12	0.0	47688.0	[26]
129. $CO + HO_2 = CO_2 + OH$	5.80E + 13	0.0	22934.0	[26]
C_2 HYDROCARBON SUBMECHANISM				
130. $C_2H_5OH(+M) = CH_2OH + CH_3(+M)$	5.94E + 23	−1.68	91163.0	This Study
Low pressure limit:	2.88E + 85	−18.9	109914.0	(g)
Troe Parameters: $a = 0.50$, $T^{***} = 200.$, $T^{*} = 890.0$, $T^{**} = 4600.0$				
Enhanced Third Body Efficiencies: $H_2O = 5.0$, $H_2 = 2.0$, $CO_2 = 3.0$, CO = 2.0				

(Continued)

Table I (Continued)

Reaction	A	b	E_a	Reference
131. $C_2H_5OH(+M) = C_2H_5 + OH(+M)$	1.25E + 23	−1.54	96005.0	This Study
Low pressure limit:	3.25E + 85	−18.81	114930.0	(g)
Troe Parameters: $a = 0.50$, $T^{***} = 300.$, $T^{*} = 900.$, $T^{**} = 5000.$				
Enhanced Third Body Efficiencies: $H_2O = 5.0$, $H_2 = 2.0$, $CO_2 = 3.0$, $CO = 2.0$				
132. $C_2H_5OH(+M) = C_2H_4 + H_2O(+M)$	2.79E + 13	0.09	66136.0	This Study
Low pressure limit:	2.57E + 83	−18.85	86452.0	(g)
Troe Parameters: $a = 0.70$, $T^{***} = 350.$, $T^{*} = 800.$, $T^{**} = 3800.$				
Enhanced Third Body Efficiencies: $H_2O = 5.0$				
133. $C_2H_5OH(+M) = CH_3HCO + H_2(+M)$	7.24E + 11	0.095	91007.0	This Study
Low pressure limit:	4.46E + 87	−19.42	115586.0	(g)
Troe Parameters: $a = 0.90$, $T^{***} = 900.$, $T^{*} = 1100.$, $T^{**} = 3500.$				
Enhanced Third Body Efficiencies: $H_2O = 5.0$				
134. $C_2H_5OH + OH = C_2H_4OH + H_2O$	1.74E + 11	0.27	600.0	This Study (h)
135. $C_2H_5OH + OH = CH_3CHOH + H_2O$	4.64E + 11	0.15	0.0	This Study
136. $C_2H_5OH + OH = CH_3CH_2O + H_2O$	7.46E + 11	0.30	1634.0	This Study
137. $C_2H_5OH + H = C_2H_4OH + H_2$	1.23E + 07	1.80	5098.0	This Study (i)
138. $C_2H_5OH + H = CH_3CHOH + H_2$	2.58E + 07	1.65	2827.0	This Study
139. $C_2H_5OH + H = CH_3CH_2O + H_2$	1.50E + 07	1.60	3038.0	This Study
140. $C_2H_5OH + O = C_2H_4OH + H_2O$	9.41E + 07	1.70	5459.0	This Study (j)
141. $C_2H_5OH + O = CH_3CHOH + H_2O$	1.88E + 07	1.85	1824.0	This Study
142. $C_2H_5OH + O = CH_3CH_2O + H_2O$	1.58E + 07	2.00	4448.0	This Study
143. $C_2H_5OH + CH_3 = C_2H_4OH + CH_4$	2.19E + 02	3.18	9622.0	This Study (k)
144. $C_2H_5OH + CH_3 = CH_3CHOH + CH_4$	7.28E + 02	2.99	7948.0	This Study
145. $C_2H_5OH + CH_3 = CH_3CH_2O + CH_4$	1.45E + 02	2.99	7649.0	This Study
146. $C_2H_5OH + HO_2 = C_2H_4OH + H_2O_2$	1.23E + 04	2.55	15750.0	This Study
147. $C_2H_5OH + HO_2 = CH_3CHOH + H_2O_2$	8.20E + 03	2.55	10750.0	This Study
148. $C_2H_5OH + HO_2 = CH_3CH_2O + H_2O_2$	2.50E + 12	0.00	24000.0	This Study
149. $CH_3CH_2O + M = CH_3HCO + H + M$	1.16E + 35	−5.89	25274.0	QRRK, 1 atm
150. $CH_3CH_2O + M = CH_3 + CH_2O + M$	1.35E + 38	−6.96	23800.0	QRRK, 1 atm
151. $CH_3CH_2O + CO = C_2H_5 + CO_2$	4.68E + 02	3.16	5380.0	(l)
152. $CH_3CH_2O + O_2 = CH_3HCO + HO_2$	4.00E + 10	0.00	1100.0	[70]
153. $CH_3CH_2O + H = CH_3 + CH_2OH$	3.00E + 13	0.00	0.0	(a)
154. $CH_3CH_2O + H = C_2H_4 + H_2O$	3.00E + 13	0.00	0.0	(a)
155. $CH_3CH_2O + OH = CH_3HCO + H_2O$	1.00E + 13	0.00	0.0	(a)
156. $CH_3CHOH + O_2 = CH_3HCO + HO_2$	4.82E + 14	0.00	5017.0	(m)
Duplicate				
$CH_3CHOH + O_2 = CH_3HCO + HO_2$	8.43E + 15	−1.20	0.0	
Duplicate				
157. $CH_3CHOH + CH_3 = C_3H_6 + H_2O$	2.00E + 13	0.00	0.0	(a)
158. $CH_3CHOH + O = CH_3HCO + OH$	1.00E + 14	0.00	0.0	(a)
159. $CH_3CHOH + H = CH_3 + CH_2OH$	3.00E + 13	0.00	0.0	(a)
160. $CH_3CHOH + H = C_2H_4 + H_2O$	3.00E + 13	0.00	0.0	(a)
161. $CH_3CHOH + HO_2 = CH_3HCO + OH + OH$	4.00E + 13	0.00	0.0	(a)
162. $CH_3CHOH + OH = CH_3HCO + H_2O$	5.00E + 12	0.00	0.0	(a)
163. $CH_3CHOH + M = CH_3HCO + H + M$	1.00E + 14	0.00	25000.0	(a)
164. $CH_3HCO + OH = CH_3CO + H_2O$	9.24E + 06	1.50	−962.0	[71]
165. $CH_3HCO + OH = CH_2HCO + H_2O$	1.72E + 05	2.40	815.0	[71]

(Continued)

Table I (Continued)

Reaction	A	b	E_a	Reference
166. $CH_3HCO + OH = CH_3 + HCOOH$	3.00E + 15	−1.076	0.0	[71]
167. $CH_3HCO + O = CH_3CO + OH$	1.77E + 18	−1.90	2975.0	(o,p)
168. $CH_3HCO + O = CH_2HCO + OH$	3.72E + 13	−0.20	3556.0	(o,p)
169. $CH_3HCO + H = CH_3CO + H_2$	4.66E + 13	−0.35	2988.0	(o,q)
170. $CH_3HCO + H = CH_2HCO + H_2$	1.85E + 12	0.40	5359.0	(o,q)
171. $CH_3HCO + CH_3 = CH_3CO + CH_4$	3.90E − 07	5.80	2200.0	(o,r)
172. $CH_3HCO + CH_3 = CH_2HCO + CH_4$	2.45E + 01	3.15	5727.0	(o,r)
173. $CH_3HCO + HO_2 = CH_3CO + H_2O_2$	2.40E + 19	−2.20	14030.0	(o,s)
174. $CH_3HCO + HO_2 = CH_2HCO + H_2O_2$	2.32E + 11	0.40	14864.0	(o,s)
175. $CH_3HCO + O_2 = CH_3CO + HO_2$	1.00E + 14	0.0	42200.0	(a)
176. $CH_2HCO + H = CH_3 + HCO$	5.00E + 13	0.0	0.0	(a)
177. $CH_2HCO + H = CH_2CO + H_2$	2.00E + 13	0.0	0.0	(a)
178. $CH_2HCO + O = CH_2O + HCO$	1.00E + 14	0.0	0.0	[26]
179. $CH_2HCO + OH = CH_2CO + H_2O$	3.00E + 13	0.0	0.0	[26]
180. $CH_2HCO + O_2 = CH_2O + CO + OH$	3.00E + 10	0.0	0.0	[26]
181. $CH_2CHO + CH_3 = C_2H_5 + CO + H$	4.90E + 14	−0.50	0.0	[26]
182. $CH_2CHO + HO_2 = CH_2O + HCO + OH$	7.00E + 12	0.00	0.0	(t)
183. $CH_2CHO + HO_2 = CH_3HCO + O_2$	3.00E + 12	0.00	0.0	(u)
184. $CH_2HCO = CH_3 + CO$	1.17E + 43	−9.83	43756.0	QRRK, 1 atm
185. $CH_2HCO = CH_2CO + H$	1.81E + 43	−9.61	45868.0	QRRK, 1 atm
186. $C_2H_6 + CH_3 = C_2H_5 + CH_4$	5.50E − 01	4.0	8300.0	[26]
187. $C_2H_6 + H = C_2H_5 + H_2$	5.40E + 02	3.5	5210.0	[26]
188. $C_2H_6 + O = C_2H_5 + OH$	3.00E + 07	2.0	5115.0	[26]
189. $C_2H_6 + OH = C_2H_5 + H_2O$	7.23E + 06	2.0	864.0	[26]
190. $C_2H_5 + H = C_2H_4 + H_2$	1.25E + 14	0.0	8000.0	[26]
191. $C_2H_5 + H = CH_3 + CH_3$	3.00E + 13	0.0	0.0	[26]
192. $C_2H_5 + H = C_2H_6$	3.00E + 13	0.0	0.0	[26]
193. $C_2H_5 + OH = C_2H_4 + H_2O$	4.00E + 13	0.0	0.0	[26]
194. $C_2H_5 + O = CH_3 + CH_2O$	1.00E + 14	0.0	0.0	[26]
195. $C_2H_5 + HO_2 = C_2H_6 + O_2$	3.00E + 12	0.0	0.0	[26]
196. $C_2H_5 + HO_2 = CH_3 + CH_2O + OH$	3.00E + 13	0.0	0.0	[26]
197. $C_2H_5 + O_2 = C_2H_4 + HO_2$	2.89E + 28	−5.40	7585.0	[72]
198. $C_2H_5 + O_2 = CH_3HCO + OH$	4.90E + 11	−0.48	8357.0	[72]
199. $C_2H_4 + OH = C_2H_4OH$	1.29E + 12	0.0	−817.0	[73]
200. $C_2H_4OH + O_2 = HOC_2H_4O_2$	1.00E + 12	0.0	−1100.0	(a)
201. $HOC_2H_4O_2 = CH_2O + CH_2O + OH$	6.00E + 10	0.0	24500.0	(a)
202. $C_2H_4 + H = C_2H_3 + H_2$	3.36E − 07	6.0	1692.0	[26]
203. $C_2H_4 + OH = C_2H_3 + H_2O$	2.02E + 13	0.0	5936.0	[26]
204. $C_2H_4 + O = CH_3 + HCO$	1.02E + 07	1.88	179.0	[26]
205. $C_2H_4 + O = CH_2HCO + H$	3.39E + 06	1.88	179.0	[26]
206. $C_2H_4 + CH_3 = C_2H_3 + CH_4$	6.62E + 00	3.70	9500.0	[26]
207. $C_2H_4 + H(+M) = C_2H_5(+M)$	1.08E + 12	0.454	1822.0	[26]
Low pressure limit:	1.11E + 34	−5.00	4448.0	
Troe Parameters: $a = 1.0$, $T^{***} = 1.0E - 15$, $T^{*} = 95.0$, $T^{**} = 200.0$				
Enhanced Third Body Efficiencies: $H_2O = 5.0$, $H_2 = 2.0$, $CO_2 = 3.0$, $CO = 2.0$				
208. $C_2H_4(+M) = C_2H_2 + H_2(+M)$	1.80E + 14	0.0	87000.0	[29]
Low pressure limit:	1.50E + 15	−0.0	55443.0	
209. $C_2H_3 + H(+M) = C_2H_4(+M)$	6.10E + 12	0.27	280.0	[29]
Low pressure limit:	9.80E + 29	−3.86	3320.0	
Troe Parameters: $a = 0.782$, $T^{***} = 208.$, $T^{*} = 2663.$, $T^{**} = 6095.$				
Enhanced Third Body Efficiencies: $H_2O = 5.0$				

(Continued)

Table I (Continued)

Reaction	A	b	E_a	Reference
210. $C_2H_3 + H = C_2H_2 + H_2$	9.00E + 13	0.0	0.0	[65]
211. $C_2H_3 + O = CH_2CO + H$	3.00E + 13	0.0	0.0	[26]
212. $C_2H_3 + O_2 = CH_2O + HCO$	1.70E + 29	−5.312	6500.0	[26]
213. $C_2H_3 + O_2 = CH_2HCO + O$	5.50E + 14	−0.611	5260.0	[26]
214. $C_2H_3 + O_2 = C_2H_2 + HO_2$	2.12E − 06	6.00	9484.0	[26]
215. $C_2H_3 + OH = C_2H_2 + H_2O$	2.00E + 13	0.0	0.0	[26]
216. $C_2H_3 + C_2H = C_2H_2 + C_2H_2$	3.00E + 13	0.0	0.0	[26]
217. $C_2H_3 + CH = CH_2 + C_2H_2$	5.00E + 13	0.0	0.0	[26]
218. $C_2H_3 + CH_3 = AC_3H_5^{\ddagger} + H$	4.73E + 02	3.7	5677.0	[26]
219. $C_2H_3 + CH_3 = C_3H_6$	4.46E + 56	−13.0	13865.0	[26]
220. $C_2H_3 + CH_3 = C_2H_2 + CH_4$	2.00E + 13	0.0	0.0	[26]
221. $C_2H_2 + OH = C_2H + H_2O$	3.37E + 07	2.0	14000.0	[26]
222. $C_2H_2 + OH = HCCOH + H$	5.04E + 05	2.3	13500.0	[26]
223. $C_2H_2 + OH = CH_2CO + H$	2.18E − 04	4.5	−1000.0	[26]
Duplicate reaction				
$C_2H_2 + OH = CH_2CO + H$	2.00E + 11	0.0	0.0	[26]
Duplicate reaction				
224. $C_2H_2 + OH = CH_3 + CO$	4.83E − 04	4.0	−2000.0	[26]
225. $HCCOH + H = CH_2CO + H$	1.00E + 13	0.0	0.0	[26]
226. $C_2H_2 + O = CH_2 + CO$	6.12E + 06	2.0	1900.0	[26]
227. $C_2H_2 + O = HCCO + H$	1.43E + 07	2.0	1900.0	[26]
228. $C_2H_2 + O = C_2H + OH$	3.16E + 15	−0.6	15000.0	[26]
229. $C_2H_2 + CH_3 = C_2H + CH_4$	1.81E + 11	0.0	17289.0	[26]
230. $C_2H_2 + O_2 = HCCO + OH$	4.00E + 07	1.5	30100.0	[26]
231. $C_2H_2 + M = C_2H + H + M$	4.20E + 16	0.0	107000.0	[26]
232. $C_2H_2 + H(+M) = C_2H_3(+M)$	3.11E + 11	0.58	2589.0	[26]
Low pressure limit:	2.25E + 40	−7.269	6577.0	[26]
Troe Parameters: a = 1.0, T^{***} = 1.0E − 15, T^{*} = 675.0, T^{**} = 1.0E + 15				
Enhanced Third Body Efficiencies: H_2O = 5.0, H_2 = 2.0, CO_2 = 3.0, CO = 2.0				
233. $CHOCHO(+M) = CH_2O + CO(+M)$	4.27E + 12	0.0	50600.0	[26]
Low pressure limit:	8.91E + 16	0.0	49200.0	[26]
234. $CHOCHO = CO + CO + H_2$	4.07E + 42	−8.5	69278.0	[26]
235. $CHOCHO + OH = HCO + CO + H_2O$	1.00E + 13	0.0	0.0	[26]
236. $CHOCHO + O = HCO + CO + OH$	7.24E + 12	0.0	1970.0	[26]
237. $CHOCHO + H = CH_2O + HCO$	1.00E + 12	0.0	0.0	[26]
238. $CHOCHO + HO_2 = HCO + CO + H_2O_2$	1.70E + 12	0.0	10700.0	[26]
239. $CHOCHO + CH_3 = HCO + CO + CH_4$	1.74E + 12	0.0	8440.0	[26]
240. $CHOCHO + O_2 = HCO + CO + HO_2$	1.00E + 14	0.0	37000.0	[26]
241. $CH_3CO(+M) = CH_3 + CO(+M)$	3.00E + 12	0.0	16722.0	[26]
Low pressure limit:	1.20E + 15	0.0	12518.0	
242. $CH_2CO + O = CO_2 + CH_2$	1.75E + 12	0.0	1350.0	[26]
243. $CH_2CO + H = CH_3 + CO$	2.71E + 04	2.75	714.0	[29]
244. $CH_2CO + H = HCCO + H_2$	2.00E + 14	0.0	8000.0	[26]
245. $CH_2CO + O = HCCO + OH$	1.00E + 13	0.0	8000.0	[26]
246. $CH_2CO + OH = HCCO + H_2O$	1.00E + 13	0.0	2000.0	[26]
247. $CH_2CO + OH = CH_2OH + CO$	3.73E + 12	0.0	−1013.0	[26]
248. $CH_2CO(+M) = CH_2 + CO(+M)$	3.00E + 14	0.0	70980.0	[26]
Low pressure limit:	3.60E + 15	0.0	59270.0	
249. $C_2H + H_2 = C_2H_2 + H$	4.09E + 05	2.39	864.3	[26]
250. $C_2H + O = CH + CO$	5.00E + 13	0.0	0.0	[26]
251. $C_2H + OH = HCCO + H$	2.00E + 13	0.0	0.0	[26]
252. $C_2H + O_2 = CO + CO + H$	9.04E + 12	0.0	−457.0	[26]

(Continued)

Table I (Continued)

Reaction	A	b	E_a	Reference
253. $HCCO + C_2H_2 = H_2CCCH + CO$	1.00E + 11	0.0	3000.0	[26]
254. $HCCO + H = CH_2(S) + CO$	1.00E + 14	0.0	0.0	[26]
255. $HCCO + O = H + CO + CO$	8.00E + 13	0.0	0.0	[26]
256. $HCCO + O = CH + CO_2$	2.95E + 13	0.0	1113.0	[26]
257. $HCCO + O_2 = HCO + CO + H$	2.50E + 08	1.0	0.0	[26]
258. $HCCO + O_2 = CO_2 + HCO$	2.40E + 11	0.0	−854.0	[26]
259. $HCCO + CH = C_2H_2 + CO$	5.00E + 13	0.0	0.0	[26]
260. $HCCO + HCCO = C_2H_2 + CO + CO$	1.00E + 13	0.0	0.0	[26]
261. $HCCO + OH = C_2O + H_2O$	3.00E + 13	0.0	0.0	[26]
262. $C_2O + H = CH + CO$	1.00E + 13	0.0	0.0	[26]
263. $C_2O + O = CO + CO$	5.00E + 13	0.0	0.0	[26]
264. $C_2O + OH = CO + CO + H$	2.00E + 13	0.0	0.0	[26]
265. $C_2O + O_2 = CO + CO + O$	2.00E + 13	0.0	0.0	[26]
C_3 HYDROCARBON SUBMECHANISM				
266. $C_3H_8(+M) = C_2H_5 + CH_3(+M)$	7.90E + 22	−1.8	88629.0	[26]
Low pressure limit:	7.24E + 27	−2.88	67448.0	
Troe Parameters: $a = 1.0$, $T^{***} = 1.0E - 15$, $T^{*} = 1500.0$, $T^{**} = 1.0E + 15$				
Enhanced Third Body Efficiencies: $H_2O = 5.0$, $H_2 = 2.0$, $CO_2 = 3.0$, $CO = 2.0$				
267. $C_3H_8 + HO_2 = NC_3H_7 + H_2O_2$	4.76E + 04	2.55	16492.0	[26]
268. $C_3H_8 + HO_2 = IC_3H_7 + H_2O_2$	9.64E + 03	2.6	13909.0	[26]
269. $C_3H_8 + OH = NC_3H_7 + H_2O$	3.16E + 07	1.8	934.0	[26]
270. $C_3H_8 + OH = IC_3H_7 + H_2O$	7.08E + 06	1.9	−159.0	[26]
271. $C_3H_8 + O = NC_3H_7 + OH$	3.73E + 06	2.4	5504.0	[26]
272. $C_3H_8 + O = IC_3H_7 + OH$	5.48E + 05	2.5	3139.0	[26]
273. $C_3H_8 + H = IC_3H_7 + H_2$	1.30E + 06	2.4	4471.0	[26]
274. $C_3H_8 + H = NC_3H_7 + H_2$	1.33E + 06	2.54	6756.0	[26]
275. $C_3H_8 + CH_3 = NC_3H_7 + CH_4$	9.04E − 01	3.65	7153.0	[26]
276. $C_3H_8 + CH_3 = IC_3H_7 + CH_4$	1.51E + 00	3.46	5480.0	[26]
277. $C_3H_8 + C_2H_3 = IC_3H_7 + C_2H_4$	1.00E + 03	3.1	8830.0	[26]
278. $C_3H_8 + C_2H_3 = NC_3H_7 + C_2H_4$	6.00E + 02	3.3	10500.0	[26]
279. $C_3H_8 + C_2H_5 = IC_3H_7 + C_2H_6$	1.51E + 00	3.46	7470.0	[26]
280. $C_3H_8 + C_2H_5 = NC_3H_7 + C_2H_6$	9.03E − 01	3.65	9140.0	[26]
281. $C_3H_8 + AC_3H_5 = C_3H_6 + NC_3H_7$	2.35E + 02	3.3	19842.0	[26]
282. $C_3H_8 + AC_3H_5 = C_3H_6 + IC_3H_7$	7.83E + 01	3.3	18169.0	[26]
283. $NC_3H_7(+M) = C_2H_4 + CH_3(+M)$	1.23E + 13	−0.1	30202.0	[26]
Low pressure limit:	5.49E + 49	−10.0	35766.0	[26]
Troe Parameters: $a = 2.17$, $T^{***} = 1.0E - 15$, $T^{*} = 251.0$, $T^{**} = 1185.0$				
Enhanced Third Body Efficiencies: $H_2O = 5.0$, $H_2 = 2.0$, $CO_2 = 3.0$, $CO = 2.0$				
284. $C_3H_6 + H(+M) = IC_3H_7(+M)$	5.70E + 09	1.16	874.0	[26]
Low pressure limit:	1.64E + 54	−11.1	9364.0	
Troe Parameters: $a = 1.0$, $T^{***} = 1.0E - 15$, $T^{*} = 260.0$, $T^{**} = 3000.0$				
Enhanced Third Body Efficiencies: $H_2O = 5.0$, $H_2 = 2.0$, $CO_2 = 3.0$, $CO = 2.0$				
285. $NC_3H_7 + O_2 = C_3H_6 + H_2O_2$	1.88E + 20	−2.69	7109.0	[72]
286. $IC_3H_7 + O_2 = C_3H_6 + H_2O_2$	3.83E + 26	−4.44	7724.0	[72]
287. $IC_3H_7 + H = C_2H_5 + CH_3$	5.00E + 13	0.0	0.0	[26]
288. $NC_3H_7 + H = C_2H_5 + CH_3$	1.00E + 14	0.0	0.0	[26]
289. $NC_3H_7 + HO_2 = C_3H_8 + O_2$	3.00E + 12	0.0	0.0	(u)
290. $IC_3H_7 + HO_2 = C_3H_8 + O_2$	3.00E + 12	0.0	0.0	(u)

(Continued)

Table I (Continued)

Reaction	A	b	E_a	Reference
291. $PC_3H_5^{\ddagger} + H = C_3H_6$	1.00E + 14	0.0	0.0	[26]
292. $SC_3H_5^{\ddagger} + H = C_3H_6$	1.00E + 14	0.0	0.0	[26]
293. $C_3H_6 = C_2H_2 + CH_4$	2.50E + 12	0.0	70000.0	[26]
294. $C_3H_6 = AC_3H_4^{\ddagger} + H_2$	3.00E + 13	0.0	80000.0	[26]
295. $C_3H_6 + HO_2 = AC_3H_5 + H_2O_2$	9.64E + 03	2.6	13910.0	[26]
296. $C_3H_6 + OH = AC_3H_5 + H_2O$	3.12E + 06	2.0	−298.0	[26]
297. $C_3H_6 + OH = SC_3H_5 + H_2O$	1.11E + 06	2.0	1451.0	[26]
298. $C_3H_6 + OH = PC_3H_5 + H_2O$	2.11E + 06	2.0	2778.0	[26]
299. $C_3H_6 + O = CH_3CHCO + H + H$	5.01E + 07	1.76	76.0	[26]
300. $C_3H_6 + O = C_2H_5 + HCO$	1.58E + 07	1.76	−1216.0	[26]
301. $C_3H_6 + O = AC_3H_5 + OH$	5.24E + 11	0.7	5884.0	[26]
302. $C_3H_6 + O = PC_3H_5 + OH$	1.20E + 11	0.7	8959.0	[26]
303. $C_3H_6 + O = SC_3H_5 + OH$	6.03E + 10	0.7	7632.0	[26]
304. $C_3H_6 + H = C_2H_4 + CH_3$	7.23E + 12	0.0	1302.0	[26]
305. $C_3H_6 + H = AC_3H_5 + H_2$	1.73E + 05	2.5	2492.0	[26]
306. $C_3H_6 + H = SC_3H_5 + H_2$	4.09E + 05	2.5	9794.0	[26]
307. $C_3H_6 + H = PC_3H_5 + H_2$	8.04E + 05	2.5	12284.0	[26]
308. $C_3H_6 + CH_3 = AC_3H_5 + CH_4$	2.22E + 00	3.5	5675.0	[26]
309. $C_3H_6 + CH_3 = SC_3H_5 + CH_4$	8.43E − 01	3.5	11656.0	[26]
310. $C_3H_6 + CH_3 = PC_3H_5 + CH_4$	1.35E + 00	3.5	12848.0	[26]
311. $C_3H_6 + HCO = AC_3H_5 + CH_2O$	1.08E + 07	1.9	17010.0	[26]
312. $CH_3CHCO + OH = CH_2CHCO + H_2O$	4.00E + 06	2.0	0.0	[26]
313. $CH_3CHCO + O = CH_2CHCO + OH$	7.60E + 08	1.5	8500.0	[26]
314. $CH_3CHCO + H = CH_2CHCO + H_2$	2.00E + 05	2.5	2500.0	[26]
315 $CH_3CHCO + H = C_2H_5 + CO$	2.00E + 13	0.0	2000.0	[26]
316. $CH_3CHCO + O = CH_3 + HCO + CO$	3.00E + 07	2.0	0.0	[26]
317. $CH_2CHCHO + OH = CH_2CHCO + H_2O$	1.00E + 13	0.0	0.0	[26]
318. $CH_2CHCHO + O = CH_2CHCO + OH$	7.24E + 12	0.0	1970.0	[26]
319. $CH_2CHCHO + O = CH_2CO + HCO + H$	5.01E + 07	1.76	76.0	[26]
320. $CH_2CHCHO + H = CH_2CHCO + H_2$	3.98E + 13	0.0	4200.0	[26]
321. $CH_2CHCHO + H = C_2H_4 + HCO$	2.00E + 13	0.0	3500.0	[26]
322. $CH_2CHCHO + O_2 = CH_2CHCO + HO_2$	3.00E + 13	0.0	36000.0	[26]
323. $CH_2CHCO = C_2H_3 + CO$	1.00E + 14	0.0	34000.0	[26]
324. $CH_2CHCO + O = C_2H_3 + CO_2$	1.00E + 14	0.0	0.0	[26]
325. $AC_3H_5 + O_2 = CH_2CHCHO + OH$	1.82E + 13	−0.41	22859.0	[26]
326. $AC_3H_5 + O_2 = AC_3H_4 + HO_2$	4.99E + 15	−1.4	22428.0	[26]
327. $AC_3H_5 + O_2 = CH_2HCO + CH_2O$	1.06E + 10	0.34	12838.0	[26]
328. $AC_3H_5 + O_2 = C_2H_2 + CH_2O + OH$	2.78E + 25	−4.8	15468.0	[26]
329. $AC_3H_5 + HO_2 = CH_2CHCH_2O + OH$	1.00E + 13	0.0	0.0	[26]
330. $AC_3H_5 + HO_2 = C_3H_6 + O_2$	3.00E + 12	0.0	0.0	[75]
331. $AC_3H_5 + OH = AC_3H_4 + H_2O$	1.00E + 13	0.0	0.0	[26]
332. $AC_3H_5 + H = AC_3H_4 + H_2$	5.00E + 13	0.0	0.0	[26]
333. $AC_3H_5 + H = C_3H_6$	1.88E + 26	−3.6	5468.0	[26]
334. $AC_3H_5 + O = CH_2CHCHO + H$	1.81E + 14	0.0	0.0	[26]
335. $AC_3H_5 + CH_3 = AC_3H_4 + CH_4$	3.02E + 12	−0.32	−131.0	[26]
336. $PC_3H_5 + O_2 = CH_3HCO + HCO$	1.09E + 23	−3.29	3892.0	[26]
337. $PC_3H_5 + O_2 = CH_3CHCO + H + O$	1.60E + 15	−0.78	3135.0	[26]
338. $PC_3H_5 + O = CH_3CHCO + H$	1.00E + 14	0.0	0.0	[26]
339. $PC_3H_5 + H = PC_3H_4 + H_2$	2.00E + 13	0.0	0.0	[26]
340. $PC_3H_5 + OH = PC_3H_4 + H_2O$	1.00E + 13	0.0	0.0	[26]
341. $PC_3H_5 + H = AC_3H_5 + H$	1.00E + 14	0.0	0.0	[26]
342. $SC_3H_5 + H = AC_3H_5 + H$	1.00E + 14	0.0	0.0	[26]
343. $SC_3H_5 + O_2 = CH_3CO + CH_2O$	1.09E + 22	−3.29	3892.0	[26]
344. $SC_3H_5 + O = CH_2CO + CH_3$	1.00E + 14	0.0	0.0	[26]

(Continued)

Table I (Continued)

Reaction	A	b	E_a	Reference
345. $SC_3H_5 + H = PC_3H_4 + H_2$	4.00E + 13	0.0	0.0	[26]
346. $SC_3H_5 + OH = PC_3H_4 + H_2O$	2.00E + 13	0.0	0.0	[26]
347. $CH_2CHCH_2O + O_2 = CH_2CHCHO + HO_2$	4.00E + 10	0.0	1100.0	(a)
348. $CH_2CHCH_2O + CO = AC_3H_5 + CO_2$	4.68E + 02	3.16	5380.0	(a)
349. $CH_2CHCH_2O + H = AC_3H_4 + H_2O$	3.00E + 13	0.0	0.0	(a)
350. $CH_2CHCHO + H(+M) = CH_2CHCH_2O(+M)$	5.40E + 11	0.454	2600.0	(a)
Low pressure limit:	1.50E + 30	−4.80	5560.0	
Troe Parameters: $a = 0.78$, $T^{***} = 94.$, $T^{*} = 1555.$, $T^{**} = 4200.$				
Enhanced Third Body Efficiencies: $H_2O = 5.0$,				
351. $AC_3H_4 + H = H_2CCCH + H_2$	2.00E + 07	2.0	5000.0	[29]
352. $AC_3H_4 + O = C_2H_4 + CO$	1.34E + 07	1.88	179.0	[26]
353. $AC_3H_4 + OH = H_2CCCH + H_2O$	1.00E + 07	2.0	1000.0	[29]
354. $AC_3H_4 + CH_3 = H_2CCCH + CH_4$	1.50E + 00	3.5	5600.0	[26]
355. $AC_3H_4 = PC_3H_4$	1.48E + 13	0.0	60401.0	[29]
356. $PC_3H_4 + H = H_2CCCH + H_2$	2.00E + 07	2.0	5000.0	[29]
357. $PC_3H_4 + O = C_2H_4 + CO$	1.50E + 13	0.0	2102.0	[26]
358. $PC_3H_4 + OH = H_2CCCH + H_2O$	1.00E + 07	2.0	1000.0	[29]
359. $PC_3H_4 + CH_3 = H_2CCCH + CH_4$	1.50E + 00	3.5	5600.0	[26]
360. $PC_3H_4 + H = CH_3 + C_2H_2$	5.12E + 10	1.0	2060.0	[29]
361. $PC_3H_4 + H(+M) = SC_3H_5(+M)$	6.50E + 12	0.0	2000.0	[26]
Low pressure limit:	8.45E + 39	−7.27	6577.0	
362. $AC_3H_4 + H(+M) = AC_3H_5(+M)$	1.20E + 11	0.69	3007.0	[26]
Low pressure limit:	5.56E + 33	−5.0	4448.0	
363. $AC_3H_4 + H(+M) = SC_3H_5(+M)$	8.49E + 12	0.0	2000.0	[26]
Low pressure limit:	1.11E + 34	−5.0	4448.0	
364. $H_2CCCH + O_2 = CH_2CO + HCO$	3.00E + 10	0.0	2868.0	[26]
365. $H_2CCCH + O = CH_2O + C_2H$	1.40E + 14	0.0	0.0	[75]
366. $H_2CCCH + H = C_3H_2 + H_2$	5.00E + 13	0.0	1000.0	[75]
367. $H_2CCCH + OH = C_3H_2 + H_2O$	2.00E + 13	0.0	0.0	[26]
368. $H_2CCCH + H(+M) = AC_3H_4(+M)$	1.66E + 15	−0.37	0.0	[25]
Low pressure limit:	3.36E + 45	−8.52	6293.0	
Enhanced Third Body Efficiencies: $H_2O = 5.0$, $H_2 = 2.0$, $CO_2 = 3.0$, $CO = 2.0$ $O_2 = 2.0$, $C_2H_2 = 2.0$				
369. $H_2CCCH + H(+M) = PC_3H_4(+M)$	1.66E + 15	−0.37	0.0	[25]
Low pressure limit:	8.78E + 45	−8.9	7974.0	
Enhanced Third Body Efficiencies: $H_2O = 5.0$, $H_2 = 2.0$, $CO_2 = 3.0$, $CO = 2.0$ $O_2 = 2.0$, $C_2H_2 = 2.0$				

(Continued)

tion found for each model compound were used and the overall measured rate constant was implemented as a constraint for H-atom abstraction from ethanol. The reaction path degeneracy associated with the number of H-atoms available for abstraction between ethanol and the model compounds were included in the branching ratio calculations. The equations used in the branching ratio determination for $C_2H_5OH + X \leftrightarrow$ Products reactions are shown below:

$$a_1a_2K_{sm}/K_{xm} = R1 \quad (1)$$

$$b_1b_2K_{pm}/K_{sm} = R2 \quad (2)$$

$$K_p = K_{overall}R2/((1/R1) + R2 + 1) \quad (3)$$

$$K_s = K_{overall}/((1/R1) + R2 + 1) \quad (4)$$

$$K_x = (K_{overall}/R1)/((1/R1) + R2 + 1) \quad (5)$$

$$K_{overall} = K_p + K_s + K_x \quad (6)$$

Table I (Continued)

Reaction	A	b	E_a	Reference
370. $C_3H_2 + O_2 = HCCO + CO + H$	2.00E + 12	0.0	1000.0	[75]
371. $C_3H_2 + O = C_2H_2 + CO$	1.00E + 14	0.0	0.0	[75]
372. $C_3H_2 + OH = C_2H_2 + HCO$	5.00E + 13	0.0	0.0	[25]

" $\rightarrow$ " indicates reverse rate not included.

$^{\alpha}$ Fall-off reaction in the Lindemann–Hinshelwood form:

$k = k_o[M]/(1 + k_o[M]/k_\infty)$

$^{\beta}$ Fall-off reaction in the Troe form:

$(k = k_o[M]/(1 + k_o[M]/k_\infty))$ F

$\log F = (1 + (\kappa/(N - d\,\kappa))^2)^{-1} \log F_{cent}$; $\kappa = \log(k_o[M]/k_\infty) + C$

$C = -0.4 - 0.67 \log F_{cent}$; $N = 0.75 - 1.27 \log F_{cent}$; $d = 0.14$

$F_{cent} = (1 - a) \exp(-T/T^{***}) + a \exp(-T/T^{*}) + \exp(-T^{**}/T)$

‡ $CH_2(s)(^1CH_2)$; iC_3H_7 (iso-C_3H_7, CH_3CHCH_3); nC_3H_7 (n-C_3H_7, $CH_2CH_2CH_3$); aC_3H_5 (allyl, CH_2CHCH_2); pC_3H_5 (2-methylvinyl, $HCCHCH_3$); sC_3H_5 (1-methylvinyl, CH_2CCH_3); aC_3H_4 (allene, H_2CCCH_2); pC_3H_4 (propyne, H_3CCCH).

(a) Estimate

(b) RRKM/Master Equation analysis performed using UNIMOL program [50].

(c) Input parameters obtained from Walch [59] for RRKM/Master Equation analysis. Calculations were performed for the 1000–2000K temperature range with an applied energy transfer value of $<\Delta E>_{down} = 500\ cm^{-1}$.

(d) Barrier height obtained from [76].

(e) Analogy to $CH_3OH + X = CH_3O + XH$ reaction where X = {OH,H}.

(f) Analogy to $CH_3CHO + X = CH_3CO + XH$ reaction where X = {OH,H,CH_3,HO_2,O}.

(g) See text.

(h) See text. Overall rate expression for $C_2H_5OH + OH$ = Products is 3.21E10 $T^{0.72}$ cm^3/mol/sec [39,43].

(i) See text. Applied $T^{2.0}$ fit to the low temperature data of Aders and Wagner [77] for $C_2H_5OH + H$ = Products rate expression extrapolation to high temperatures.

(j) See text. Overall rate expression for $C_2H_5OH + O$ = Products is 6.0E5 $T^{2.46}$ exp(−931 k/T) cm^3/mol/sec [78]. Branching ratio of 0.351 exp(1489 K/T) [78] was used for $k_{C_2H_5OH+O=CH_3CHOH+OH}/k_{C_2H_5OH+O=CH_3CH_2OH+OH}$ since no rate constant measurements exist for the $CH_3OH + O = CH_3O + OH$ reaction.

(k) Applied $T^{3.3}$ fit to the low temperature data of Gray and Herod [42] for $C_2H_5OH + CH_3$ = Products rate expression extrapolation to high temperatures. The rate expressions from curve B are 1.6E2 $T^{3.21}$ exp(−4869 K/T) cm^3/mol/sec for $C_2H_5OH + CH_3 = C_2H_4OH + CH_4$; 8.37E2 $T^{3.02}$ exp(−4027 K/T) cm^3/mol/sec for $C_2H_5OH + CH_3 = CH_3CHOH + CH_4$; and 3.62E2 $T^{2.95}$ exp(−3908 K/T) cm^3/mol/sec for $C_2H_5OH + CH_3 = CH_3CH_2O + CH_4$.

(l) Analogy to $CH_3O + CO$ reaction.

(m) Analogy to $CH_2OH + O_2$ reaction.

(n) A-factor reduced by a factor of 1.5.

(o) Branching ratios were obtained by treating the relative rates of H-atom abstraction as described in the text. The rate expressions used for aldehydic H-atom (CH_2O) abstraction and secondary H-atom (C_3H_8) abstraction were respectively taken from Baulch [79] and Marinov [26]. Model compounds selected were formaldehyde (CH_2O) and propane (C_3H_8).

(p) Overall rate expression for $CH_3HCO + O$ = Products is 5.84E12 exp(−910 K/T) cm^3/mol/sec [79].

(q) Overall rate expression for $CH_3HCO + H$ = Products is 4.095E9 $T^{1.16}$ exp(−1210 K/T) cm^3/mol/sec [79].

(r) Overall rate expression for $CH_3HCO + CH_3$ = Products is 1.987E − 6 $T^{5.6}$ exp(−1240 K/T) cm^3/mol/sec [79].

(s) Overall rate expression for $CH_3HCO + HO_2$ = Products is 3.01E12 exp(−6000 K/T) cm^3/mol/sec [79].

(t) Analogy to $CH_3 + HO_2 = CH_3O + OH$.

(v) Analogy to $CH_3 + HO_2 = CH_4 + O_2$ [65] and a $C_3H_5 + H_5 + HO_2 = C_3H_6 + O_2$ [74].

K_{pm} = rate constant for abstracting a primary hydrogen (H_p) in the model compound (e.g., propane)

K_{sm} = rate constant for abstracting a secondary hydrogen (H_s) in the model compound (e.g., propane and methanol)

K_{xm} = rate constant for abstracting a hydrogen from the hydroxyl group (H_x) in the model compound (e.g., methanol)

K_p = rate constant for abstracting a primary hydrogen (H_p) in ethanol

K_s = rate constant for abstracting a secondary hydrogen (H_s) in ethanol

K_x = rate constant for abstracting a hydrogen from the hydroxyl (OH) group (H_x) in ethanol

a_1 = The number of hydrogens found on the hydroxyl group (H_x) divided by the number of secondary hydrogens (H_s) in the model compound (e.g., methanol)

a_2 = The number of secondary hydrogens (H_x) divided by the number of hydrogens found on the hydroxyl group (H_x) in ethanol

Table II Thermodynamic Properties for Selected Species Units: kcal/mol for ΔH_f, cal/mol/K for S and C_p

Species	ΔH_f(298 K)	S(298 K)	C_p(300 K)	C_p(400 K)	C_p(500 K)	C_p(600 K)	C_p(800 K)	C_p(1000 K)	C_p(2500 K)
HO_2	3.50	54.77[b]	8.40[b]	8.92	9.42	9.90	10.72	11.34	12.09
CH_2[a]	93.50	46.71	8.19	8.57	8.93	9.28	9.93	10.52	11.75
$CH_2(s)$[a]	102.50	45.10	7.91	8.33	8.72	9.11	9.83	10.49	11.86
CH_2OH	−2.10[c]	58.87[b]	11.32[b]	12.94	14.38	15.62	17.54	18.79	20.95
C_2H[d]	135.0	49.55	8.90	9.63	10.22	10.72	11.54	12.18	13.31
C_2H_3[a]	70.40	55.50	9.88	11.37	12.82	14.20	16.70	18.74	21.83
C_2H_5[a]	28.73	59.02	11.85	14.44	16.81	18.98	22.70	25.64	30.20
HCOH[a]	23.33	55.42	9.83	12.88	15.17	16.85	18.89	19.84	20.65
HCOOH[e]	−90.47	59.47	10.95	13.04	14.96	16.68	19.44	21.37	23.47
CH_2HCO[d]	6.00	64.00	13.18	15.15	16.96	18.60	21.30	23.34	26.35
CHOCHO[a]	−50.60	68.16	14.90	17.51	19.69	21.48	24.15	25.89	28.10
$HOC_2H_4O_2$[f]	−38.60	84.71	21.34	24.77	27.71	30.25	34.42	37.74	43.67
IC_3H_7[a]	21.51	68.88	16.90	20.76	24.51	27.81	33.39	37.73	44.35
NC_3H_7[a]	24.05	69.16	17.18	21.71	25.54	28.81	34.00	37.91	44.36
AC_3H_5[†a]	38.64	64.73	16.07	19.55	22.72	25.53	29.99	32.89	37.43
PC_3H_5[a]	64.75	68.74	15.54	18.56	21.44	24.12	28.65	31.68	36.13
SC_3H_5[a]	61.09	69.24	15.45	18.38	21.21	23.89	28.50	31.61	36.09
CH_2CHCH_2O[a]	22.40	69.59	17.12	21.25	24.75	27.73	32.39	36.44	41.11
CH_2CHCHO[f]	−16.05	67.40	16.37	20.06	23.20	25.86	29.99	32.94	37.18
CH_2CHCO[a]	14.85	68.08	15.24	18.46	21.15	23.38	26.79	29.15	32.51
CH_3CHCO[a]	−20.06	67.75	17.63	20.72	23.39	25.71	29.42	32.19	36.43
PC_3H_4[d]	45.77	58.89	14.52	17.06	19.40	21.54	25.16	27.90	31.79
AC_3H_4[d]	47.63	57.94	14.25	16.97	19.46	21.71	25.45	28.20	32.06
H_2CCCH[d]	83.04	61.48	15.84	17.74	19.48	21.01	23.43	25.01	27.55
C_3H_2[d]	129.6	64.81	14.93	16.10	16.91	17.55	18.72	19.74	21.22
C_2H_5OH[e]	−56.15	67.05	15.67	19.31	22.84	25.96	30.59	34.15	39.53
C_2H_4OH[f]	−8.20	68.19	15.48	18.84	21.70	24.11	27.87	30.58	34.73
CH_3CHOH[f]	−10.30	62.69	14.64	17.64	20.37	22.84	26.98	30.13	34.72
CH_3CH_2O[f]	−4.10	62.21	14.08	17.72	20.85	23.53	27.75	30.80	35.32

[†] aC_3H_5 (allyl, CH_2CHCH_2); pC_3H_5 (n-C_3H_5, 1-propenyl, CH_3CHCH); sC_3H_5 (i-C_3H_5, 2-propenyl, CH_3CCH_2);
[a] (Marinov, [26]) [b] (CHEMKIN Thermodynamic Database, [32]) [c] See Text [d] [81] [e] (Burcat and McBride, [33]) [f] Group Additivity/ Difference method

b_1 = The number of secondary hydrogens (H_s) divided by the number of primary hydrogens (H_p) in the model compound (e.g., propane)
b_2 = The number of primary hydrogens (H_p) divided by the number of secondary hydrogens (H_s) in ethanol
R1 = ratio of rate constants from the model compound (e.g., methanol) corrected for the number of H-atoms available for abstraction in ethanol
R2 = ratio of rate constants from the model compound (e.g., propane) corrected for the number of H-atoms available for abstraction in ethanol
$K_{overall}$ = the total rate constant for $C_2H_5OH + X \leftrightarrow$ Products, where X = {OH, O, H, and CH_3}

A sample calculation is presented to walk the reader through the several steps required in this branching ratio estimation method. The overall rate expression for $C_2H_5OH + OH \leftrightarrow$ Products was obtained by using the rate coefficient measurements of Hess and Tully [39] in the 293–750 K temperature range and the shock tube results of Bott and Cohen [43] around 1200 K. The curve fitted rate expression of ($K_{overall}$ =) 3.21E10 $T^{0.72}$ cm^3/mol/sec was obtained from the data acquired in the two studies, where T is temperature in units of Kelvin. The relative branching ratio between the secondary hydrogen and the hydrogen on the hydroxyl group in ethanol was obtained with methanol as the model compound. Tsang [44] performed a detailed literature review and theoretical analysis work on the $CH_3OH + OH \leftrightarrow$ Products reaction. The branching ratio expression obtained from the Tsang

study for $CH_3OH + OH \leftrightarrow CH_2OH + H_2O$ and $CH_3OH + OH \leftrightarrow CH_3O + H_2O$ was (K_{sm}/K_{xm} =) 0.2703 exp (1020 K/*T*). The ratio of the rate constants from the methanol model compound corrected for the number of H-atoms available (i.e., $a_1 = 1/3$, $a_2 = 2/1$) for abstraction in ethanol yields (R1 =) (1/3)(2/1)(0.2703 exp(1020K/T)) or 0.4055 exp(1020 K/*T*). The relative branching ratio between the primary and secondary hydrogens in ethanol was obtained with propane as the model compound. Cohen [45] performed a detailed literature review and theoretical analysis work on the $C_3H_8 + OH \leftrightarrow$ Products reaction. The rate expressions obtained from the Cohen study for $C_3H_8 + OH \leftrightarrow nC_3H_7 + H_2O$ and $C_3H_8 + OH \leftrightarrow iC_3H_7 + H_2O$ were (K_{pm} =) 3.16E7 $T^{1.8}$ exp (−470 K/*T*) cm³/mol/sec and (K_{sm} =) 7.08E6 $T^{1.9}$ exp(80 K/*T*) cm³/mol/sec, respectively. The ratio of the rate constants from the propane model compound corrected for the number of H-atoms available for abstraction in ethanol yields (R2 =) (2/6)(3/2) (4.463E0 $T^{-0.10}$ exp(−550 K/*T*)) or 2.2315E0 $T^{-0.10}$ exp(−550 K/*T*). This information allows equations (3)–(5) to be solved, and the rate constants and branching ratios are obtained for the three distinct sites of H-atom abstraction from ethanol by the OH radical.

$C_2H_5OH + OH \longrightarrow$ Products

The calculated branching ratio values (i.e., $K_p/K_{overall}$, $K_s/K_{overall}$, and $K_x/K_{overall}$) are shown in Figure 2 along with the direct measurements and indirect determinations of the branching ratios for the $C_2H_5OH + OH \leftrightarrow$ Products reaction. The numerical results show a branching ratio value for $K_p/K_{overall} = k_{C_2H_5OH + OH \leftrightarrow CH_3CHOH + H_2O}/k_{overall}$ of 0.72 at 300 K. This value is in very good agreement with the direct product study of Meier et al. [38]. Meier used mass spectrometry to show that $C_2H_5OH + OH \leftrightarrow CH_3CHOH + H_2O$ accounted for 75 ± 15% of the overall reaction rate at 300 K. Around 600 K, Hess and Tully [39] monitored the decay rates of ^{18}OH and ^{16}OH radicals in the presence of ethanol ($C_2H_5{}^{16}OH$) to determine the rate constant contribution from $C_2H_5OH + OH \leftrightarrow C_2H_4OH$ (or CH_2CH_2OH) + H_2O. This product channel lead to the formation of $CH_2CH_2{}^{16}OH$ whereupon the ^{16}OH radical is regenerated by the fast dissociation reaction $CH_2CH_2{}^{16}OH \leftrightarrow C_2H_4 + {}^{16}OH$. They found the measured rate constant for the reaction of ^{18}OH radical with ethanol is ca. 18% higher than that measured for the ^{16}OH reaction with ethanol. Therefore, the $C_2H_5OH + OH \leftrightarrow C_2H_4OH + H_2O$ product channel accounted for approximately 15%–20% of the total rate constant. This study's branching ratio determination at 600K suggests a value around

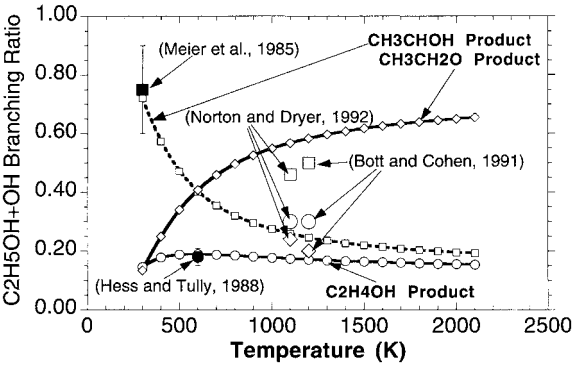

Figure 2 The $C_2H_5OH + OH \leftrightarrow$ Products branching ratio values are calculated per text discussion for the 300–2000 K temperature range. Solid symbols refer to experimental data, open symbols refer to chemical kinetic modeling/indirect determination of the branching ratios. Squares are CH_3CHOH branching ratio data. Circles are C_2H_4OH branching ratio data. Diamonds are CH_3CH_2O branching ratio data.

19% for $K_s/K_{overall} = k_{C_2H_5OH + OH \leftrightarrow C_2H_4OH + H_2O}/k_{overall}$ that is in excellent agreement to the Hess and Tully experimental finding. Two indirect determinations of the branching ratios for $C_2H_5OH + OH \leftrightarrow$ Products were presented by Bott and Cohen [43], and Norton and Dryer [6]. Bott and Cohen performed transition state theory (TST) calculations by constraining the branching flux at 298 K for the $C_2H_5OH + OH \leftrightarrow CH_3CHOH + H_2O$ channel at 75%, and assuming $C_2H_5OH + OH \leftrightarrow CH_3CH_2O + H_2O$ has a similar activation energy barrier as $CH_3OH + OH \leftrightarrow CH_3O + H_2O$. The constrained TST calculations showed $C_2H_5OH + OH$ producing C_2H_4OH: CH_3CHOH:CH_3CH_2O products by the approximate split of 30%:56%:14% at 600 K and 30%:46%:24% in the 1000–1200 K temperature range. The Bott and Cohen theoretical determination of the $C_2H_5OH + OH \leftrightarrow C_2H_4OH + H_2O$ branching ratio at 600 K overpredicted the Hess and Tully measurement by a factor of 1.5–2.0. However, their high temperature branching ratios agree with the numerical modeling work on flow reactor ethanol oxidation kinetics by Norton and Dryer (30%:50%:20% at 1100 K). This study's branching ratio value of ca. 17% at 1100 K for $C_2H_5OH + OH \leftrightarrow C_2H_4OH + H_2O$ is approximately a factor of two lower than the Bott and Cohen, and Norton and Dryer branching ratio determinations. There is also a fairly large discrepancy between the branching values selected for the CH_3CHOH and CH_3CH_2O product channels as well. This study

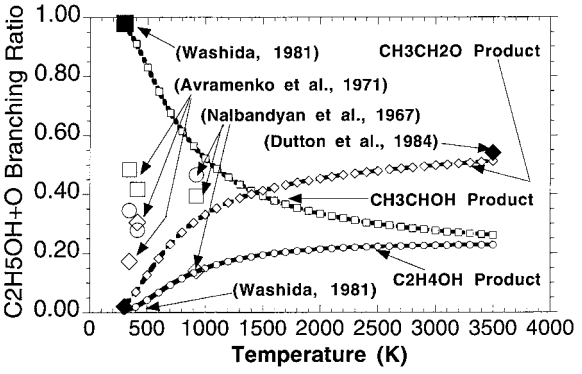

Figure 3 The $C_2H_5OH + O \leftrightarrow$ Products branching ratio values as calculated per text discussion for the 300–2000 K temperature range. Solid symbols refer to experimental data, open symbols refer to chemical kinetic modeling/indirect determination of the branching ratios. Squares are CH_3CHOH branching ratio data. Circles are C_2H_4OH branching ratio data. Diamonds are CH_3CH_2O branching ratio data.

advocates the dominance of the CH_3CH_2O product channel at high temperatures with branching ratio values of ca. 55–65% in the 1000–2000 K temperature range, and a small relative contribution from the CH_3CHOH product channel of ca. 19–27% in the 1000–2000 K temperature range. The extrapolated $C_2H_5OH + OH \leftrightarrow C_2H_4OH + H_2O$ branching ratio values to the high temperature condition are considered to be reliable.

$C_2H_5OH + O \longrightarrow$ Products

In Figure 3, the branching ratio values are shown for the $C_2H_5OH + O \leftrightarrow$ Products reaction. Direct measurements and indirect determinations of the branching ratios are also noted for comparison. The numerical results at 300 K indicate branching ratio values of 0.98 for $K_p/K_{overall} = k_{C_2H_5OH+O \leftrightarrow CH_3CHOH+H_2O}/k_{overall}$ and 0.02 for $K_x/K_{overall} = k_{C_2H_5OH+O \leftrightarrow CH_3CH_2O+H_2O}/k_{overall}$. These values are in very good agreement with the direct product study of Washida [40]. Washida used photoionization mass spectrometry to show that $C_2H_5OH + O \leftrightarrow CH_3CHOH + OH$ and $C_2H_5OH + O \leftrightarrow CH_3CH_2O + OH$ accounted for 98–100% and 0.0–2.0% respectively of the overall rate of reaction at 300 K. In another study, Dutton and co-workers [41] examined the relative importance of the H-atom abstraction sites between the O—H and C—H groups in ethanol. They used laser-induced fluorescence under crossed-molecular beam conditions to determine the $C_2H_5OH + O$ branching ratio. The $C_2H_5OD + O$ reaction was studied by monitoring the OH and OD fluorescence signals, and by knowing the OH and OD transition probabilities the relative reactivity of the abstractable H-atom sties could be determined. Their work indicated that H-atom abstraction from the hydroxyl group by O-atom was 2.2 times faster than from the C—H group at a translational temperature of 3500 K. However, these results must be corrected as an additional source of OD would be produced through the reaction sequence of $C_2H_5OD + O \leftrightarrow CH_2CH_2OD + OH$ and $CH_2CH_2OD \leftrightarrow C_2H_4 + OD$ as previously noted by Hess and Tully's mechanistic studies of $C_2H_4OH \leftrightarrow C_2H_4 + OH$ above 500 K. This implies that H-atom abstraction from the hydroxyl group by O-atom is approximately 1.2 times faster than abstraction from the C—H group at 3500 K. The empirical approach shows very good agreement with the Dutton branching ratio for the CH_3CH_2O channel at 3500 K and suggests confidence in this study's $C_2H_5OH + O \leftrightarrow CH_3CH_2O + OH$ branching ratios over the 300–3500 K temperature range. Indirect studies on the $C_2H_5OH + O$ branching ratios were conducted in the 343–413K temperature range by Avramenko and Kolensikova [46] and at 923 K by Nalbandyan et al. [47]. Avramenko determined that the C_2H_4OH:CH_3CHOH:CH_3CH_2O product ratio varied from 35%:48%:17% at 343 K to 28%:42%:30% at 413 K in their brief communications paper. Nalbandyan indicated a product ratio of 47%:39%:14% at 923 K. These results do not compare well with this study's empirically derived branching ratios.

$C_2H_5OH + CH_3 \longrightarrow$ Products

There has been one direct and indirect study on the role of methyl radical abstracting an H-atom from the three specific abstraction sites of ethanol. Gray and Herod [42] measured the rates of methyl radical attack on the H-atom sites found in the hydroxyl and the alkyl groups in ethanol by examining three isotopically different ethanol's. They found the methylene group was the most reactive site, and the methyl group was the least reactive site at 423 K. Their results showed branching ratios of 5%:75%:20% corresponding to C_2H_4OH:CH_3CHOH:CH_3CH_2O formation. In this study, fair agreement of the empirically derived branching ratios to the Gray and Herod direct study is shown as curve B in Figure 4. A branching ratio of 13%:60%:27% for C_2H_4OH:CH_3CHOH:CH_3CH_2O formation at 423 K was calculated. However, the calculated branching fraction to the $CH_3CHOH + CH_4$ products is outside the error bound prescribed by this study for the Gray and Herod measurement, and further improvement is suggested. A new branching ratio

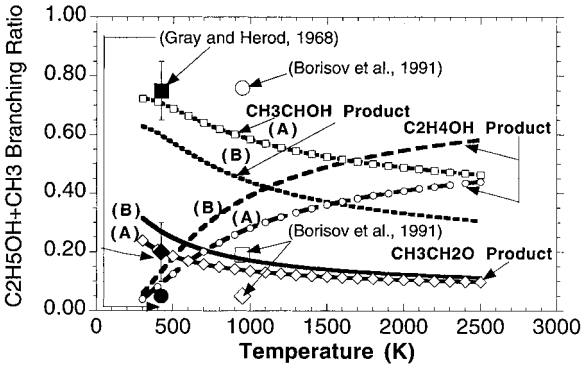

Figure 4 The $C_2H_5OH + CH_3 \leftrightarrow$ Products branching ratio values as calculated per text discussion for the 300–2000 K temperature range. Solid symbols refer to experimental data, open symbols refer to chemical kinetic modeling/indirect determination of the branching ratios. Squares are CH_3CHOH branching ratio data. Circles are C_2H_4OH branching ratio data. Diamonds are CH_3CH_2O branching ratio data.

evaluation, shown as curve A, used the k_{144}/k_{145} (see Table II) ratio from the low temperature rate constant measurements of Gray and Herod [42]. The curve A results show (1) better agreement with Gray and Herod measured branching ratios, (2) the $C_2H_5OH + CH_3 \leftrightarrow CH_3CH_2O + CH_4$ branching fraction remains essentially the same as curve B, and that (3) a 0.10–0.15 change in value between curve A and B is found for the other two channels especially at the higher temperatures.

The detailed chemical kinetic modeling work on ethanol pyrolysis in a static reactor by Borisov et al. [5] showed the $C_2H_5OH + CH_3 \leftrightarrow$ Products reaction was important for describing the product profiles measured at nearly one atmosphere and 800–1100 K. Best agreement with the product profiles was obtained when using branching ratios of 76%:19%:5% for C_2H_4OH:CH_3CHOH:CH_3CH_2O at 950 K. This study's branching ratio value of ca. 28% (curve A) at 950 K for $K_p/K_{overall} = k_{C_2H_5OH + CH_3 \leftrightarrow C_2H_4OH + CH_4}/k_{overall}$ is in poor agreement with the 76% branching ratio value determined by Borisov. This disagreement is due to the omission of the $C_2H_5OH(+M) \leftrightarrow C_2H_4 + H_2O(+M)$ reaction in the Borisov detailed chemical kinetic model. The inclusion of the ethanol dehydration reaction to the Borisov mechanism would bring their branching fraction for $k_{C_2H_5OH + CH_3 \leftrightarrow C_2H_4OH + CH_4}/k_{C_2H_5OH + CH_3 \leftrightarrow \text{Products}}$ in line with this study's value.

This study recommends using the calculated branching ratios as shown in curve A in Figure 4. The curve A representation is preferred as the Gray and Herod branching ratio measurement was reproduced, and suggests some degree of credibility to the extrapolated values at elevated temperatures. The $C_2H_5OH + CH_3 \leftrightarrow CH_3CH_2O + CH_4$ branching ratio values in curve A or B are very similar especially at elevated temperatures, and these branching ratios are considered to be reliable. Further measurements at higher temperatures would help confirm these branching ratio choices.

$C_2H_5OH + H \longrightarrow$ Products

The branching ratio estimation procedure was also adopted for H-abstraction reactions involving C_2H_5OH and H-atom. There have been no direct branching ratio studies for $C_2H_5OH + H \leftrightarrow$ Products, although Norton and Dryer provide an indirect branching ratio determination from chemical kinetic modeling. Their modeling efforts showed a branching ratio of 30%:50%:20% for C_2H:OH:CH_3CHOH:CH_3CH_2O formation at 1100 K. Figure 5 shows a branching ratio value of 26%:54%:20% at 1100 K that is in fortuitous agreement with the Norton and Dryer branching ratio findings.

$C_2H_5OH + HO_2 \longrightarrow$ Products

The branching ratio estimation procedure could not be carried out for the H-abstraction reactions involving C_2H_5OH and the HO_2 radical. This is due to a lack of rate constant measurements for the overall $C_2H_5OH + HO_2 \leftrightarrow$ Products reaction, and a lack of

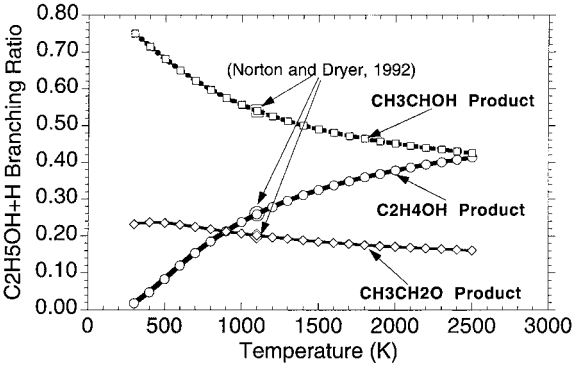

Figure 5 The $C_2H_5OH + H \leftrightarrow$ Products branching ratio values as calculated per text discussion for the 300–2000 K temperature range. Solid symbols refer to experimental data, open symbols refer to chemical kinetic modeling/indirect determination of the branching ratios. Squares are CH_3CHOH branching ratio data. Circles are C_2H_4OH branching ratio data. Diamonds are CH_3CH_2O branching ratio data.

rate constant measurements for the model compound reaction, $CH_3OH + HO_2 \leftrightarrow CH_3O + H_2O_2$. Instead, this study assumed rate expression assignments to $C_2H_5OH + HO_2 \leftrightarrow CH_3CHOH + H_2O_2$ and $C_2H_5OH + HO_2 \leftrightarrow C_2H_4OH + H_2O_2$ as 8.20E + 3 $T^{2.55}$ exp(−5410 K/T) cm^3/mol/sec and 1.23E + 4 $T^{2.55}$ exp(−7927 K/T) cm^3/mol/sec, respectively. In absence of direct rate constant measurements, these estimates are highly uncertain.

The $C_2H_5OH + HO_2 \leftrightarrow CH_3CHOH + H_2O_2$ rate expression was developed by assuming this reaction had rate constants similar to the $CH_3OH + HO_2 \leftrightarrow CH_2OH + H_2O_2$ reaction. The $T^{2.55}$ expression was taken from Tsang's analysis of $C_3H_8 + HO_2 \leftrightarrow$ Products [48] and i-$C_4H_{10} + HO_2 \leftrightarrow$ Products [49]. The remaining parameters were selected to fit the $CH_3OH + HO_2 \leftrightarrow CH_2OH + H_2O_2$ rate constants in the 750–900 K temperature range. The $CH_3OH + HO_2 \leftrightarrow CH_2OH + H_2O_2$ rate constants were taken from Held and Dryer's high pressure methanol oxidation modeling study [82]. The $C_2H_5OH + HO_2 \leftrightarrow C_2H_4OH + H_2O_2$ rate expression was based on the rate expression of $C_2H_5OH + HO_2 \leftrightarrow CH_3CHOH + H_2O_2$. A probable error of ±3.0 kcal/mol is attributed to the activation energy for $C_2H_5OH + HO_2 \leftrightarrow C_2H_4OH + H_2O_2$.

RRKM/Master Equation Calculations for the Ethanol Decomposition Reactions

In order to determine the degree of falloff and the estimate of the high pressure limit rate constant for the $C_2H_5OH(+M) \leftrightarrow CH_2OH + CH_3(+M)$ and $C_2H_5OH(+M) \leftrightarrow C_2H_5 + OH(+M)$ bond fission reactions, RRKM/Master equation theory calculations [50] were performed using the hindered rotational Gorin Model [51]. The Gorin model assumes that the internal modes of the transition state are vibrations and rotations of the separated radical fragments, and the four low frequency bending modes associated with the breaking bond are considered to be two 2-dimensional hindered rotations of the independent radical fragments. The transition state is located at the top of the centrifugal barrier. The vibration frequencies and moments of inertia for ethanol were obtained from the thermodynamic properties study by Green [52]. The transition state vibrational frequencies for C—C bond fission were assigned by using the frequencies of the

Table III Molecular and Transition State Properties Used in RRKM/Master Equation Analysis of the $C_2H_5OH \leftrightarrow CH_3 + CH_2OH$ and $C_2H_5OH \leftrightarrow C_2H_5 + OH$ Decomposition Reactions

$C_2H_5OH \leftrightarrow CH_3 + CH_2OH$
Transition State: $CH_3 \cdot CH_2OH$
Critical Energy: 86.7 kcal/mol[a]
Frequencies (degeneracy): 573,607,950,1091, 1341,1396(2),1459,1623,2844,3960,3044,3162(2),3650[b]
Inactive External Rotation (cm^{-1}): 0.104 (symmetry = 1,dimension = 2)
Active External Rotation (cm)$^{-1}$): 0.696 (symmetry = 1,dimension = 1)
Internal (cm^{-1}): 6.95(symmetry = 3,dimension = 1), 0.897(1,2), 9.57(1,2)

$C_2H_5OH \leftrightarrow C_2H_5 + OH$
Transition State: $C_2H_5 \cdot OH$
Critical Energy: 91.8 kcal/mol[a]
Frequencies (degeneracy): 540,784,975,1138,1175,1366,1440(3),2842,2920,2987,3033,3112,3730[b,c]
Inactive External Rotation (cm^{-1}): 0.093 (1,2)
Active External Rotation (cm)$^{-1}$): 0.828 (3,1)
Internal (cm^{-1}): 6.09(1,1), 0.726(1,2), 19.29(1,2)

Ground State: C_2H_5OH
Frequencies (degeneracy): (263)[d],311,427,801,1040,1067,1104,1242,1270,1320,1391,1456(3),2789(3),3689[e]
Inactive External Rotation (cm^{-1}): 0.284 (1,2)
Active External Rotation (cm^{-1}): 1.213 (1,1)
Internal (cm^{-1}): 6.46(3,1)

Lennard-Jones Parameters and Molecular Weight

C_2H_5OH[f]:	ϵ/K_B = 362.6 K	σ = 4.53 Å	Molecular Weight = 46.0 g/gmol
Argon[g]:	ϵ/K_B = 136.5 K	σ = 3.3 Å	Molecular Weight = 39.95 g/gmol

[a] This Study. [b] [33]. [c] [53]. [d] Replaced low frequency vibration with free internal rotation. [e] [52]. [f] [80]. [g] [32].

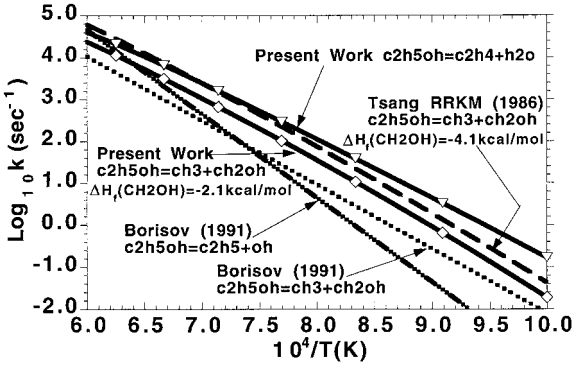

Figure 6 Comparison of this study's rate constants to data of Tsang [44] and Borisov et al. [5] for the $C_2H_5OH(+M) \leftrightarrow CH_3 + CH_2OH(+M)$ reaction at 1 atm. This study's $C_2H_5OH(+M) \leftrightarrow C_2H_4 + H_2O(+M)$ rate constants at 1 atm along with Borisov's $C_2H_5OH(+M) \leftrightarrow C_2H_5 + OH(+M)$ reaction kinetics are also included. Note: Tsang's high pressure limit rate constant [62] for $C_2H_5OH \leftrightarrow CH_3 + CH_2OH$ along with thermochemistry [44,65] were used in the RRKM derivation.

methyl radical [33] and the CH_2OH radical [33]. The transition state vibrational frequencies for the C—O bond fission reaction were assigned by using the frequencies of the ethyl radical [33] and the hydroxyl radical [53]. The fragment moments of inertia for rotation normal to the molecular axis were taken from [33] and [53]. The complete listing of parameters used in the RRKM/Master Equation calculations for $C_2H_5OH(+M) \leftrightarrow CH_2OH + CH_3(+M)$ and $C_2H_5OH(+M) \leftrightarrow C_2H_5 + OH(+M)$ are given in Table III.

Particular attention was paid to $C_2H_5OH(+M) \leftrightarrow CH_3 + CH_2O(+M)$ since this reaction was found to be one of the most sensitive reactions under shock tube conditions in the Egolfopoulos et al. and Natarajan/Bhaskaran studies as well as in the present work. The RRKM calculations were performed by consideration of three adjustable parameters: (i) the rotational constant for external and internal rotation, (ii) the critical energy, and (iii) the energy transferred per collision. A series of MOPAC PM3 [54] calculations were undertaken in order to obtain the geometry of the nearly separated fragments for the CH_3—CH_2OH complex at the top of the centrifugal barrier. These calculations allowed the rotational constants to be determined through examination of the Van der Waal repulsions of the rotating fragments. The CH_2OH heat of formation was allowed to vary from −2.1 kcal/mol [55] to −4.1 kcal/mol [32] when adjusting the critical energy and fitting the shock tube data. Best agreement was attained with a heat of formation (at 298 K) value of −2.1 (kcal/mol for CH_2OH, and this corresponded to a final critical energy value of 86.7 kcal/mol in the RRKM calculations. The energy transferred per collision value was determined to be 500 cm^{-1} in agreement with Tsang's earlier determination of $<\Delta E_{down}>$ for methanol and propane bond fission decomposition at these temperatures [44,48].

The high and low pressure limit rate constants along with the Troe parameters obtained from the RRKM/Master Equation theory calculations for $C_2H_5OH(+M) \leftrightarrow CH_3 + CH_2OH(+M)$ are

$$k_{130}^{\infty} = 5.71\text{E}23\ T^{-1.68} \exp(-47511\ \text{K}/T)\ (\text{s}^{-1})$$

$$k_{130}^{\circ} = 3.11\text{E}85\ T^{-18.84} \times \exp(-56917\ \text{K}/T)\ (\text{cm}^3/\text{mol/sec})$$

$$F_{\text{cent}} = 0.5 \exp(-T/500\ \text{K}) + 0.5 \exp(-T/825\ \text{K}) + \exp(-6100\ \text{K}/T)$$

Figure 6 shows a comparison of this study's $C_2H_5OH(+M) \leftrightarrow CH_3 + CH_2OH(+M)$ unimolecular rate constant at 1 atm with the Borisov [5] and Tsang [44] 1 atm rate expressions in the 1000 K $< T <$ 1700 K range. The Borisov rate expression and Tsang's RRKM evaluation of ethanol decomposition to methyl and hydroxymethylene differ by approximately one order of magnitude. This study's $C_2H_5OH(+M) \leftrightarrow CH_3 + CH_2OH(+M)$ rate expression agrees with Tsang's work to within a factor of two and agrees with Borisov et al. to within a factor of five. If the CH_2OH heat of formation value at 298 K were to be lowered from the present value of −2.1 kcal/mol to −4.1 kcal/mol, then this study's $C_2H_5OH(+M) \leftrightarrow CH_3 + CH_2OH(+M)$ rate constants would nearly lie on top of the Tsang evaluation. In Figure 7, rate constant comparisons at 2.0 bar are

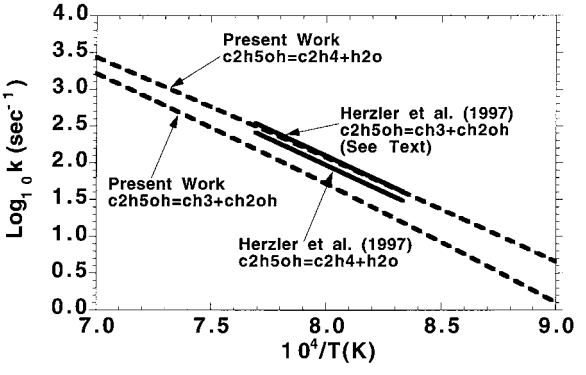

Figure 7 Comparison of this study's rate constants at 2.0 bar against data of Herzler, Manion, and Tsang [56] for $C_2H_5OH(+M) \leftrightarrow CH_3 + CH_2OH(+M)$ and $C_2H_5OH(+M) \leftrightarrow C_2H_4 + H_2O(+M)$ reactions.

shown between this study's $C_2H_5OH(+M) \leftrightarrow CH_3 + CH_2OH(+M)$ rate expression and preliminary measurements made by Herzler, Manion, and Tsang [56]. This study underpredicted the measured rate constants in the 1200–1300 K temperature range by approximately a factor of three; however, this difference may be largely attributed to the uncertainty in the measured rate constants and branching ratio for the $C_2H_5OH(+M) \leftrightarrow CH_3 + CH_2OH(+M)$ and $C_2H_5OH(+M) \leftrightarrow C_2H_4 + H_2O(+M)$ reactions. This study's $C_2H_5OH(+M) \leftrightarrow CH_3 + CH_2OH(+M)$ rate constants are in reasonable accord with Tsang's RRKM analysis and the recent measurements by Herzler et al. Therefore, the suggested rate parameters are considered acceptable.

The $C_2H_5OH(+M) \leftrightarrow C_2H_5 + OH(+M)$ rate constant calculations were performed in the same manner as described for $C_2H_5OH(+M) \leftrightarrow CH_3 + CH_2OH(+M)$. The high and low pressure limit rate constants along with the Troe parameters obtained from RRKM/Master Equation theory for $C_2H_5OH(+M) \leftrightarrow C_2H_5 + OH(+M)$ are

$$k_{131}^{\infty} = 1.25E23\ T^{-1.54} \exp(-48317\ K/T)\ (s^{-1})$$

$$k_{131}^{\circ} = 3.25E85\ T^{-18.8} \times \exp(-57891\ K/T)\ (cm^3/mol/sec)$$

$$F_{cent} = 0.5 \exp(-T/300\ K) + 0.5 \exp(-T/900\ K) + \exp(-5000\ K/T)$$

An energy transfer per collision value $<\Delta E_{down}> = 500\ cm^{-1}$ was applied in the rate constant analysis.

Additional RRKM/Master Equation theory calculations were carried out to examine the role of H_2O and H_2 elimination reactions in the ethanol decomposition process. The input parameters required for these calculations are shown in Table IV. The H_2O and H_2 elimination reactions are complex fission reactions that involve a four-centered transition state. Benson's rules for transition state frequencies [34] were applied, and a critical energy was selected to match the literature reviewed critical and activation energies. These critical energies are 64.0–67.0 kcal/mol [57,58] and 91.9 kcal/mol [59,60] respectively for

Table IV Molecular and Transition State Properties Used in RRKM/Master Equation Analysis of the $C_2H_5OH \leftrightarrow CH_2H_4 + H_2O$ and $C_2H_5OH \leftrightarrow CH_3HCO + H_2$ Decomposition Reactions

$C_2H_5OH \leftrightarrow C_2H_4 + H_2O$
Transition State: $C_2H_4 \cdot H_2O$
Critical Energy: 64.9 kcal/mol[a]
Frequencies (degeneracy): 335,400,700(4),1000(2),1150(2),1300,1450(2),2200(2),3100(4),3700[b]
Inactive External Rotation (cm^{-1}): 0.284 (symmetry = 1,dimension = 2)
Active External Rotation $(cm)^{-1}$): 1.213 (symmetry = 1,dimension = 1); Optical Isomer = 2

$C_2H_5OH \leftrightarrow CH_3HCO + H_2$
Transition State: $CH_3HCO \cdot H_2$
Critical Energy: 91.9 kcal/mol[c]
Frequencies (degeneracy): 585,800,1000(2),1150(4),1400,1450(2),2200(2),3100(4)[b]
Inactive External Rotation (cm^{-1}): 0.284 (1,2)
Active External Rotation (cm^{-1}): 1.213 (1,1); Optical Isomer = 1

Ground State: C_2H_5OH
Frequencies (degeneracy): 263,311,427,801,1040,1067,1104,1242,1270,1320,1391,1456(3),2789(3),3689[d]
Inactive External Rotation (cm^{-1}): 0.284 (1,2)
Active External Rotation (cm^{-1}): 1.213 (1,1); Optical Isomer = 1

Lennard-Jones Parameters and Molecular Weight

C_2H_5OH[e]:	ϵ/K_B = 362.6 K	σ = 4.53 Å	Molecular Weight = 46.0 g/gmol
Argon[f]:	ϵ/K_B = 136.5 K	σ = 3.3 Å	Molecular Weight = 39.95 g/gmol

[a] This Study and [56,57,58,61]. [b] [34]. [c] Assumed critical energy for $C_2H_5OH \leftrightarrow CH_3HCO + H_2$ had same value as $CH_3OH \leftrightarrow CH_2O + H_2$ [59]. [d] [52]. [e] [80]. [f] [32].

H_2O and H_2 elimination from ethanol. A high pressure limit activation energy for H_2O elimination from ethanol has been suggested to be 66.0 kcal/mol–66.2 kcal/mol [56,61]. The transition state frequencies for the C—C·O and C—C˙—O bends are very low and uncertain. An initial value of 240 cm^{-1} was used for the transition state C—C·O bending motion, but this value was later adjusted upward to 335 cm^{-1} to obtain modeling agreement with the ethylene measurements in the jet-stirred and turbulent flow reactors. This point will be further discussed in the modeling results of the jet-stirred and turbulent flow reactors. Likewise for the $C_2H_5OH \leftrightarrow CH_3HCO + H_2$ decomposition reaction, the transition state C—C˙—O bend frequency was adjusted upward by the same factor from an initial value of 420 cm^{-1} to 585 cm^{-1}. The calculated high and low pressure rate constants and the associated Troe parameters using an energy transfer per collision value of $<\Delta E_{down}> = 500\ cm^{-1}$ for $C_2H_5OH(+M) \leftrightarrow C_2H_4 + H_2O(+M)$ are

$$k_{132}^{\infty} = 2.79E13\ T^{0.09} \exp(-33284\ K/T)\ (s^{-1})$$

$$k_{132}^{\circ} = 2.57E83\ T^{-18.85} \times \exp(-43509\ K/T)\ (cm^3/mol/sec)$$

$$F_{cent} = 0.3 \exp(-T/350\ K) + 0.7\exp(-T/800\ K) + \exp(-3800\ K/T)$$

The $C_2H_5OH \leftrightarrow C_2H_4 + H_2O$ high pressure limit is compared to other known data for this reaction as shown in Figure 8. There is a fair amount of scatter amongst the derived rate constants. The Tsang [62] and the Zhitneva and Pshezhetskii [60] rate constants were derived by examining the rate constants measured for analogous reactions that eliminate water. The Tsang and Zhitneva activation energy choices were higher than those found in the recent Butkovskaya and Setser [57,58] analysis and the Herzler, Manion, and Tsang [56] recommendation. Butkovskaya and Setser performed ab initio and RRKM calculations on ethanol and the four-centered dehydration transition state step using MP2(FC)/6–31*G*(d) and MP2(Full)/6–311*G*(d,p) levels of theory. Their RRKM results were based on the ab initio data, and the calculated high pressure limit rate constant is substantially faster than Tsang and Zhitneva, but in excellent agreement with Herzler. This study's high pressure limit is in agreement with the Butkovskaya and Setser study and the Herzler et al. recommendation. In Figure 7, rate constant comparisons at 2.0 bar are shown between this study's $C_2H_5OH(+M) \leftrightarrow C_2H_4 + H_2O(+M)$ rate expression and measurements made by Herzler, Manion, and Tsang [56]. The agreement between the two studies is fairly remarkable, and suggests that this study's $C_2H_5OH(+M) \leftrightarrow C_2H_4 + H_2O(+M)$ rate expression is entirely reasonable.

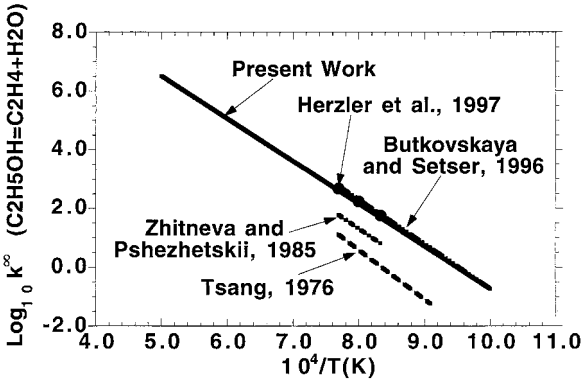

Figure 8 Comparison of this study's high pressure limit for the $C_2H_5OH \leftrightarrow C_2H_4 + H_2O$ reaction against data of Herzler, Manion, and Tsang [56], Butkovskaya and Setser [58], Zhitneva et al. [60], and Tsang [62].

The multi-parameter rate expression for $C_2H_5OH(+M) \leftrightarrow CH_3HCO + H_2(+M)$ was calculated and shown to be

$$k_{133}^{\infty} = 7.24E11\ T^{0.095} \times \exp\ (-45801\ K/T)\ (s^{-1})$$

$$k_{133}^{\circ} = 4.46E87\ T^{-19.42} \times \exp(-58171\ K/T)\ (cm^3/mol/sec)$$

$$F_{cent} = 0.1 \exp(-T/900K) + 0.9 \exp(-T/1100\ K) + \exp(-3500\ K/T)$$

$$<\Delta E_{down}> = 500\ cm^{-1}$$

A comparison of the high pressure limit rate expressions for C_2H_5OH decomposition to $CH_3 + CH_2OH$, $C_2H_5 + OH$, $C_2H_4 + H_2O$, $CH_3CHOH + H$, $C_2H_4OH + H$, and $CH_3HCO + H_2$ products is shown in Figure 9. High pressure rate expressions for C_2H_5OH decomposition to $CH_3CHOH + H$ and $CH_2CH_2OH + H$ products were obtained from Tsang [62] and these pathways are shown to be unimportant. Interestingly, the ethanol dehydration step was found to be dominant for temperatures below 1100 K due to the lower activation energy barrier, while simple C—C and C—O bond rupture reactions dominate at the higher temperatures as entropic processes become important. However, when fall-off considerations at 1.0 atm are taken into account as shown in Figure 6, the $C_2H_5OH(+M) \leftrightarrow C_2H_4 + H_2O(+M)$ reaction is the dominant decomposition reaction over $C_2H_5OH(+M) \leftrightarrow CH_3 + CH_2OH(+M)$. This is pri-

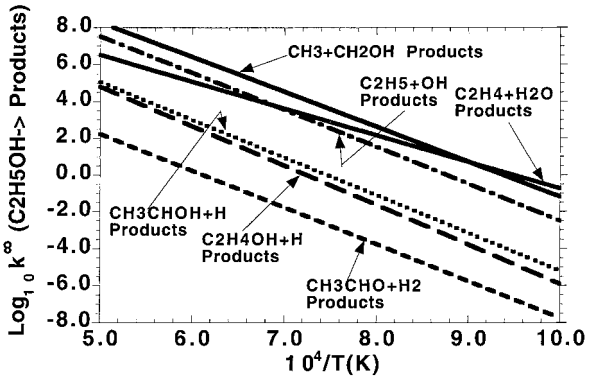

Figure 9 Comparison of the high pressure limit rate constants for Ethanol decomposition to Products. The rate constants for the $C_2H_4OH + H$ and $CH_3CHOH + H$ product channels were taken from Tsang [62].

marily due to the lower critical energy found in the water elimination reaction, which allows for higher low-pressure limit rate constants to be calculated than those found in the C—C or C—O bond fission steps. Ethanol decomposition to $CH_3 + CH_2OH$ is favored over $C_2H_5 + OH$ since the C—C bond strength is weaker than the C—O bond strength by approximately 5.0 kcal/mol. The molecular elimination of H_2 from ethanol is extremely slow as a high energy barrier, and the loss of the C—O internal rotation at the transition state limits its rate of decomposition relative to the other ethanol destruction pathways.

DISCUSSION OF THE NUMERICAL MODELING RESULTS

Modeling Ignition Delay in Shock Tubes

Natarajan and Bhaskaran were the first researchers to investigate the ignition of ethanol-oxygen-argon gas mixtures behind reflected shock waves. Experiments were performed for the 1300–1700K temperature range, for pressures of 1.0 and 2.0 atm, and for equivalence ratios of 0.5, 1.0, and 2.0 [2]. In the experimental investigation, the ignition event was identified by the first visible light emission, whereupon their experimental ignition delay data were found to be correlated by the global expression of $\tau_{vis} = 1.0 \times 10^{-15}$ exp(19221 K/T)$[C_2H_5OH]^{0.1}[O_2]^{-0.75}[Ar]^{-0.25}$, where τ_{vis} is in seconds, and reactant concentrations are in mol/cm^3.

Dunphy and Simmie [3,20] later investigated ethanol ignition behind reflected shock waves over a parameter space similar to Natarajan and Bhaskaran. Ethanol and oxygen mixtures diluted in argon were investigated for equivalence ratios of 0.25–2.0, pressures of 1.8 to 4.6 bar, and 1100–1900K. In the experimental study, the ignition event was defined as the time to maximum emission of 366 nm radiation, which is attributed to CO_2 chemiluminescence. The overall results for ignition delay time were correlated by the expression $\tau max_{co—o}(sec) = 1.0 \times 10^{-14}$ exp(15500 K/T)$[C_2H_5OH]^{-0.315}$ $[O_2]^{-0.78}[Ar]^{0.259}$.

The numerical simulations of the ignition delay behind reflected shock waves were conducted using the SENKIN code assuming an adiabatic, constant volume system. This assumption allows for both the temperature and pressure to increase during reaction. In modeling the Dunphy and Simmie experiments, the theoretical ignition delay was defined as the time required to reach a maximum in the product of the CO and O-atom concentration (= $\tau max_{co—o}$). This definition was assumed to be equated with the maximum 366 nm radiation occurrence in their experiments. The computational results using this definition are shown as the solid line in Figures 10–12. The modeling of the Natarajan and Bhaskaran experiments is difficult since the experimental ignition delay was defined as the first visible light emission. In modeling their data, the theoretical ignition delay was defined in two ways. The computed ignition delay time was assumed to be either the maximum in the product CO and O-atom concentrations (= $\tau max_{co—o}$) as indicated by the solid line or when the computed OH concentration reached 2.0×10^{-9} mol/cc as indicated by the dashed line in Figures 13–15.

In Figures 10–15, the experimental data of Dunphy/Simmie and Natarajan/Bhaskaran are presented and these data are compared to the numerical computations. The numerical simulations are shown to be in good agreement with both data sets, especially when

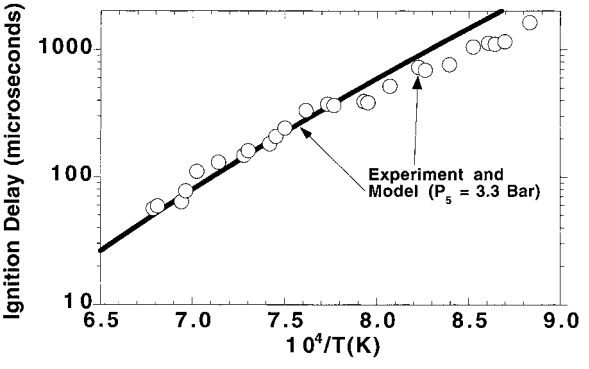

Figure 10 Comparison between experimental (symbols) shock tube ignition delay data as investigated by Dunphy and Simmie [3] and the numerical calculations (lines) using the chemical kinetic model. Experimental conditions: 1.25% C_2H_5OH, 7.50% O_2, and 91.25% Argon (equivalence ratio = 0.5), and 3.3 bar.

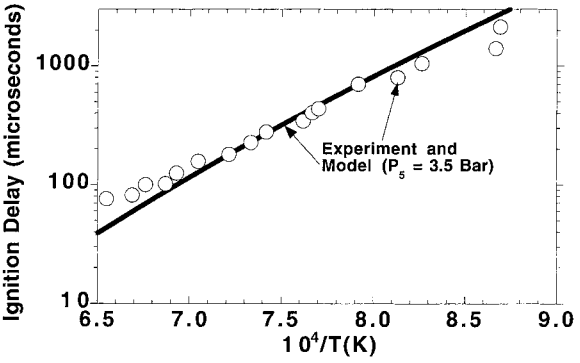

Figure 11 Comparison between experimental (symbols) shock tube ignition delay data as investigated by Dunphy and Simmie [3] and the numerical calculations (lines) using the chemical kinetic model. Experimental conditions: 1.25% C_2H_5OH, 3.75% O_2, and 95.0% Argon (equivalence ratio = 1.0), and 3.5 bar.

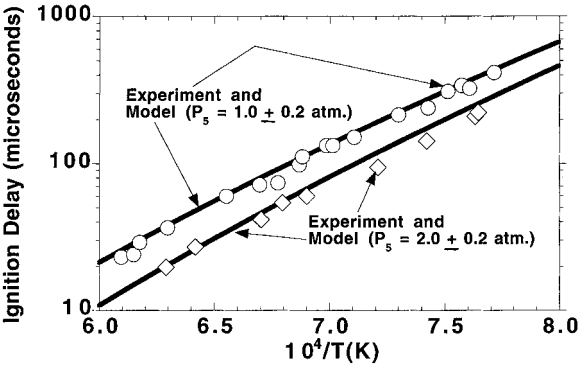

Figure 13 Comparison between experimental (symbols) shock tube ignition delay data as investigated by Natarajan and Bhaskaran [2] and the numerical calculations (lines) using the chemical kinetic model. Experimental conditions: 1.43% C_2H_5OH, 8.57% O_2, and 90% Argon (equivalence ratio = 0.5), and 1.0 ± 0.2 and 2.0 ± 0.2 atm.

considering the uncertainty associated with the theoretical ignition delay definition. The thermal decomposition of ethanol has been previously suggested as the most likely initiation reaction for these conditions [63], and was determined to be very important in this study as noted by the sensitivity analysis results shown in Figure 16. Sensitivity analysis was carried out only for the Dunphy and Simmie data sets since they are representative of the conditions examined by Natarajan/Bhaskaran.

Sensitivity analysis was performed by perturbing the forward and reverse rate constants per reaction by a factor of two, thereby leaving the thermodynamic equilibrium constant unaffected. The sensitivity coefficient was then determined by taking the natural logarithm of the ignition delay time, calculated with the perturbed reaction kinetics divided by the baseline unperturbed reaction kinetics, ignition delay time; whereupon the sensitivity coefficient expression is represented by

$$S = -\ln(\tau_{\text{perturbed kinetics}}/\tau_{\text{unperturbed kinetics}}),$$

τ = ignition delay time

If the sensitivity coefficient exhibits a positive value that would indicate an increase in the overall reactivity of the chemical system, a negative value would imply a decrease in the overall reactivity. Large sensitivity coefficient values indicate a strong influence of the reaction kinetics on ethanol ignition delay. The sen-

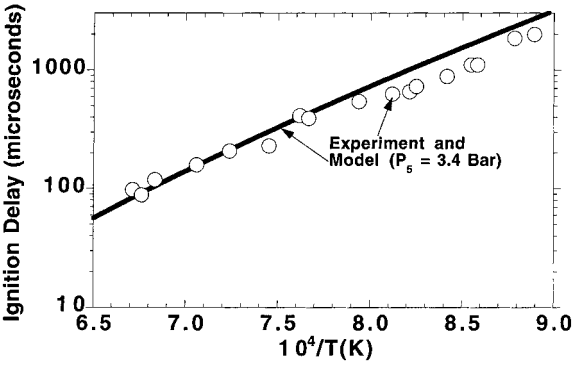

Figure 12 Comparison between experimental (symbols) shock tube ignition delay data as investigated by Dunphy and Simmie [3] and the numerical calculations (lines) using the chemical kinetic model. Experimental conditions: 2.5% C_2H_5OH, 3.75% O_2, and 93.25% Argon (equivalence ratio = 2.0), and 3.4 bar.

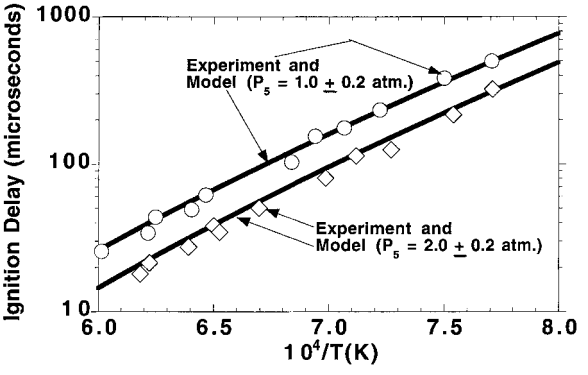

Figure 14 Comparison between experimental (symbols) shock tube ignition delay data as investigated by Natarajan and Bhaskaran [2] and the numerical calculations (lines) using the chemical kinetic model. Experimental conditions: 2.5% C_2H_5OH, 7.5% O_2, and 90% Argon (equivalence ratio = 1.0), and 1.0 ± 0.2 and 2.0 ± 0.2 atm.

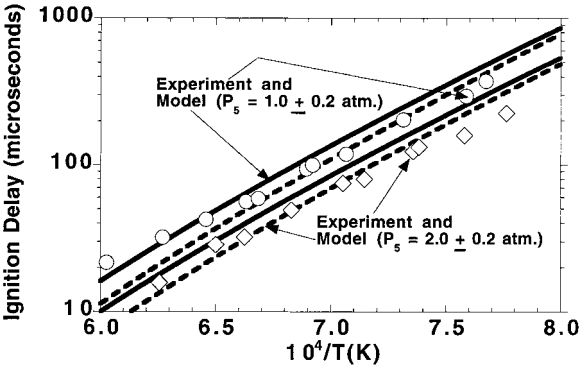

Figure 15 Comparison between experimental (symbols) shock tube ignition delay data as investigated by Natarajan and Bhaskaran [2] and the numerical calculations (solid and dashed lines) using the chemical kinetic model. Experimental conditions: 4.0% C_2H_5OH, 6.0% O_2, and 90% Argon (equivalence ratio = 2.0), and 1.0 ± 0.2 and 2.0 ± 0.2 atm. See text.

sitivity analysis study was conducted at ethanol-oxygen equivalence ratios of 0.5, 1.0, and 2.0 at 3.4 bar and 1429 K. The results are shown in Figure 16. For the conditions found in the Dunphy and Simmie experiments, the six most sensitive reactions are, in order of their peak sensitivity coefficients for $\tau max_{co—o}$,

$$(\downarrow)\ C_2H_5OH(+M) \longleftrightarrow CH_3 + CH_2OH(+M) \quad (130)$$
$$(\downarrow)\ C_2H_5OH(+M) \longleftrightarrow C_2H_5 + OH(+M) \quad (131)$$
$$(\downarrow)\ O + OH \longleftrightarrow O_2 + H \quad (2)$$
$$(\downarrow)\ CH_3 + HO_2 \longleftrightarrow CH_3O + O \quad (27)$$
$$(\downarrow)\ HCO + M \longleftrightarrow H + CO + M \quad (112)$$
$$(\uparrow)\ H + HO_2 \longleftrightarrow H_2 + O_2 \quad (7)$$

The (↑) and (↓) signs indicate whether the factor of two increase in the reaction rate increases, (↑), or decreases, (↓), $\tau max_{co—o}$. The most sensitive reaction at Φ = 0.5 and Φ = 1.0 is the well-known branching reaction $H + O_2 \leftrightarrow OH + O$ (↓). The relative sensitivity of the other reactions may be understood on the basis of their effect on the supply of H-atoms to the branching reaction. This is shown by the H-atom consuming reaction, $H + HO_2 \leftrightarrow O_2 + H_2$ (↑), and the H-atom producing reactions, $HCO + M \leftrightarrow H + CO + M$ (↓) and $CH_3CH_2O + M \leftrightarrow CH_3HCO + H + M$ (↓).

The first and second most sensitive reactions, at Φ = 2.0, are the chain initiating steps $C_2H_5OH(+M) \leftrightarrow CH_3 + CH_2OH(+M)$ (↓) and $C_2H_5OH(+M) \leftrightarrow C_2H_5 + OH(+M)$ (↓). The homolytic scission of the C—C and C—O bond initiates the radical pool growth necessary for ignition. This is demonstrated by the following consecutive reactions,

$$\begin{aligned} C_2H_5OH(+M) &\longrightarrow CH_3 + CH_2OH(+M) \\ CH_2OH + O_2 &\longrightarrow CH_2O + HO_2 \\ CH_3 + HO_2 &\longrightarrow CH_3O + OH \\ CH_3O(+M) &\longrightarrow CH_2O + H(+M) \\ H + O_2 &\longrightarrow OH + O \end{aligned} \quad (1)$$

$$\begin{aligned} C_2H_5OH(+M) &\longrightarrow C_2H_5 + OH(+M) \\ C_2H_5(+M) &\longrightarrow C_2H_4 + H(+M) \\ H + O_2 &\longrightarrow OH + O \end{aligned} \quad (2)$$

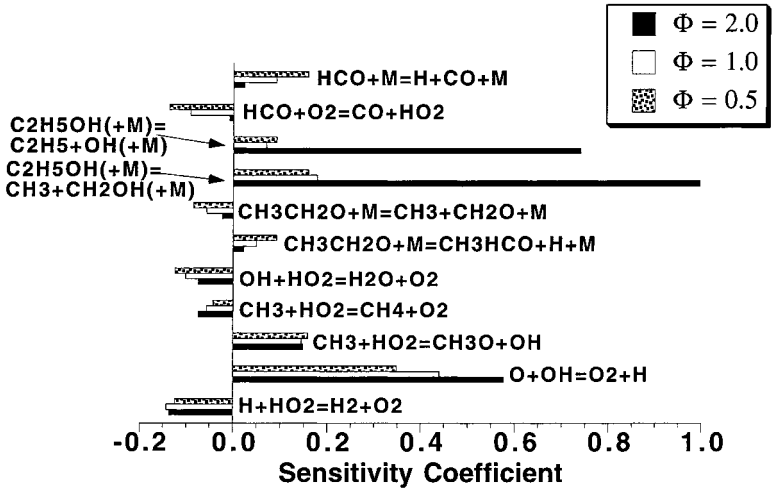

Figure 16 First order sensitivity coefficients of the most important reactions for ignition delay of lean, stoichiometric, and rich ethanol gas mixtures based on the Dunphy and Simmie [3] shock tube conditions. Nominal pressure of 3.4 bar and temperature of 1429 K.

Modeling agreement to the Dunphy/Simmie and Natarajan/Bhaskaran experimental data sets could not be achieved without the use of the $C_2H_5OH(+M) \leftrightarrow CH_3 + CH_2OH(+M)$ reaction. Interestingly, the $C_2H_5OH(+M) \leftrightarrow C_2H_4 + H_2O(+M)$ reaction consumed a greater fraction of the ethanol than $C_2H_5OH(+M) \leftrightarrow CH_3 + CH_2O(+M)$, yet $C_2H_5OH(+M) \leftrightarrow C_2H_4 + H_2O(+M)$ always exhibited a negligible sensitivity coefficient compared to $C_2H_5OH(+M) \leftrightarrow CH_3 + CH_2OH(+M)$. This finding further demonstrates the importance of homolytic scission of the C—C (and C—O) bond(s) on initiating the radical pool growth for ignition.

The $CH_3 + HO_2 \leftrightarrow CH_3O + OH$ ($\downarrow$) reaction followed by CH_3O decomposition to CH_2O + H-atom is the main supply route for H-atoms and OH radicals. The sensitivity shown for this chain propagating reaction is primarily due to the alternative product pathway which leads to chain termination, $CH_3 + HO_2 \leftrightarrow CH_4 + O_2$ ($\uparrow$). The availability of this alternative reaction path makes the rate constants for $CH_3 + HO_2 \leftrightarrow CH_3O + OH$ and $CH_3 + HO_2 \leftrightarrow CH_4 + O_2$ important.

The $H + HO_2 \leftrightarrow H_2 + O_2$ ($\uparrow$) and $OH + HO_2 \leftrightarrow H_2O + O_2$ ($\uparrow$) reactions exhibit sensitivity primarily due to their influence on the OH radical pool. The OH radical's primary role is to oxidize the ethanol. The $H + HO_2 \leftrightarrow H_2 + O_2$ reaction limits the amount of OH radical produced from the alternative product pathway, $H + HO_2 \leftrightarrow OH + OH$. The chain terminating nature of this reaction slows the ethanol destruction rate. The $OH + HO_2 \leftrightarrow H_2O + O_2$ reaction is chain terminating and removes OH from the radical pool, slowing ethanol oxidation via $C_2H_5OH + OH \leftrightarrow$ Products.

Modeling Laminar Burning Velocities in Freely Propagating Flames

Gulder [17] investigated laminar flame speeds (S_u) of ethanol-air gas mixtures in a constant volume bomb for a wide range of unburned gas pressures (P_u), 0.1–0.8 MPa, unburned gas temperatures (T_u), 300–500 K, and equivalence ratios 0.7–1.4. The maximum uncertainty determined for the measured laminar flame speeds was ±2.0 cm/sec based on the uncertainities associated in the measured unburned gas mixture temperature (±3.0 K), unburned gas mixture pressure (±1%), and equivalence ratio (±0.015). The 0.1 MPa experimental data showed the maximum ethanol-air laminar flame speed occurred around an equivalence ratio of 1.075 with a value of 47 cm/sec. At elevated pressures, the ethanol-air laminar speeds decreased with pressure while exhibiting the following pressure dependencies with equivalence ratio, $S_u = S_{u,ref}(P)^{-0.17\sqrt{\phi}}$ for $\phi \geq 1.0$, and $S_u = S_{u,ref}(P)^{-0.17\sqrt{\phi}}$ for $\phi \leq 1.0$, where 300 K and 0.1 MPa are the reference conditions. This study used the laminar flame speed data acquired at 0.1 and 0.2 MPa for model validation.

Egolfopoulos et al. [4] used the counterflow twin-flame technique to measure laminar flame speeds at 1 atm pressure, with a temperature range of 363–453K, and an equivalence ratio range of 0.55–1.8. They report a maximum uncertainty of ±10% to their flame

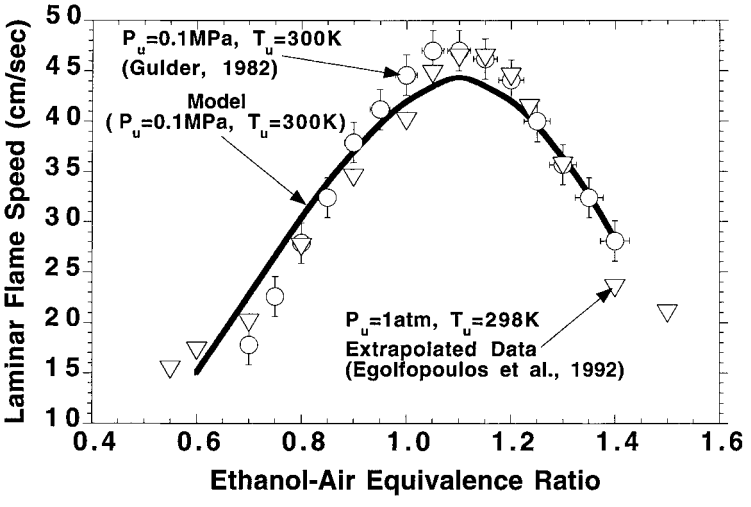

Figure 17 Comparison between experimental (symbols) laminar flame speeds as a function of equivalence ratio as investigated by Gulder [17] and the numerical calculations (lines) using the detailed chemical kinetic model. The extrapolated data of Egolfopoulos et al. [4] is also shown for comparison. Model calculations were performed at $P_u = 0.1$ MPa and $T_u = 300$ K.

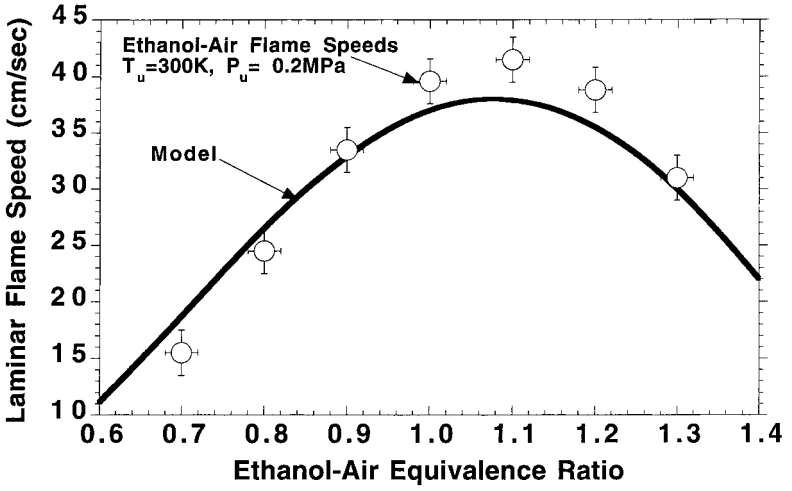

Figure 18 Comparison between experimental (symbols) laminar flame speeds as a function of equivalence ratio as investigated by Gulder [17] and the numerical calculations (lines) using the detailed chemical kinetic model. Experimental conditions were $P_u = 0.2$ MPa and $T_u = 300$ K.

speed data. This study used the experimental data acquired at 453 K for model validation.

Figures 17–19 show the comparison of the numerical computations with the experimental data obtained from the combustion bomb and the counterflow twin flame. In Figure 17, the extrapolated laminar flame speed data of Egolfopoulos from flame speed measurements performed at higher unburned gas temperatures 363–453K, are also shown for comparison. The numerical results at 0.1 MPa show a slight flame speed overprediction of ca. 3.0 cm/sec in the 0.70–0.75 equivalence ratio range, and an underprediction of ca. 2.0 cm/sec in the 1.05–1.15 equivalence ratio range. Otherwise, very good agreement with the experimental data is shown at the other equivalence ratios. The model shows good agreement with the experimental measurements at 0.2 MPa as shown in Figure 18. The model is able to correctly predict the location of the maximum flame speed for unburned gas pressures of 0.1 MPa and 0.2 MPa. Numerical calculations performed for the unburned gas temperature of 453 K and 1 atm is shown in Figure 19. The model predicts the

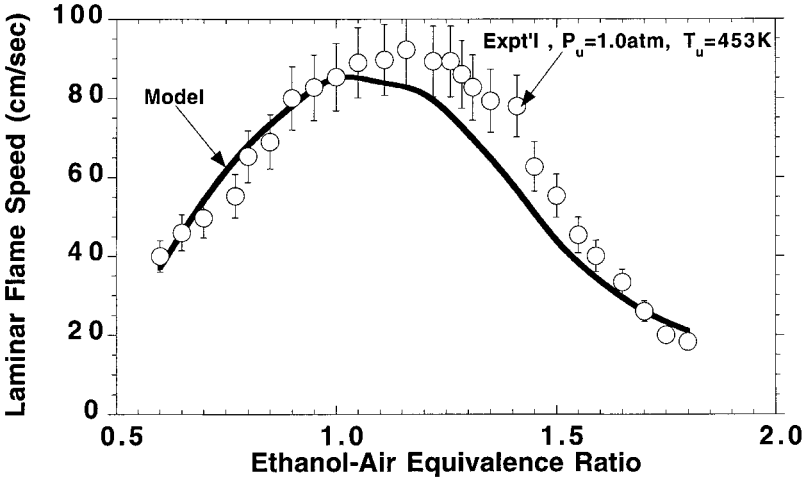

Figure 19 Comparison between experimental (symbols) laminar flame speeds as a function of equivalence ratio as investigated by Egolofopoulos et al. [4] and the numerical calculations (lines) using the detailed chemical kinetic model. Experimental conditions were $P_u = 1.0$ atm and $T_u = 453$ K.

laminar flame speeds very well for the 0.55–1.2 and 1.6–1.8 equivalence ratio ranges, but underpredicts the measurements in the 1.2–1.6 equivalence ratio range.

Sensitivity analysis was performed at an unburned gas temperature of 453 K and 1.0 atm in order to determine the influence of those chemical reactions and their associated kinetic rate constants on the mass burning rate, $M = p_u S_u$, where p_u refers to the density of the unburned gas mixture. The normalized sensitivity coefficients were calculated using the expression, $(A_i/M)(\Delta M/\Delta A_i)$, where A_i is the pre-exponential factor of the *i*th kinetic rate constant. The results of the sensitivity analysis are presented in Figure 20. At $\phi = 0.6$, $CO + OH \leftrightarrow CO_2 + H$ is the most sensitive reaction found in lean ethanol-air freely propagating laminar flames, followed in order by $H + O_2 \leftrightarrow OH + O$, $HCO + M \leftrightarrow H + CO + M$, $H + HO_2 \leftrightarrow OH + OH$, $CH_2HCO \leftrightarrow CH_2CO + H$, and $HO_2 + H \leftrightarrow H_2 + O_2$. As the equivalence ratios become progressively richer, the $H + O_2 \leftrightarrow OH + O$ reaction exhibits the greatest sensitivity, while the $CO + OH \leftrightarrow CO_2 + H$ reaction decreases dramatically in sensitivity. The reduction in the $CO + OH \leftrightarrow CO_2 + H$ sensitivity coefficient is due to a greater number of reaction intermediates competing effectively for the OH radical at progressively richer conditions. This phenomena constrains H-atom production from this reaction, and consequently limits its impact on promoting flame propagation.

The sensitivity analysis results indicate the importance of H-atom sources and sinks when modeling ethanol-air laminar flame speeds. Reactions such as $CO + OH \leftrightarrow CO_2 + H$, $HCO + M \leftrightarrow H + CO + M$, $CH_2HCO \leftrightarrow CH_2CO + H$, and $C_2H_2 + H(+M) \leftrightarrow C_2H_3(+M)$ exhibit positive sensitivity coefficients, thereby enhancing the flame speed or the overall reactivity of the chemical system since they are the primary producers of H-atoms. The $H + O_2 \leftrightarrow OH + O$ and $H + HO_2 \leftrightarrow OH + OH$ reactions, although consumers of H-atoms, also exhibit a positive sensitivity coefficient as they produce reactive OH and O radicals that are necessary to consume ethanol and its reaction intermediates. The $H + CH_3(+M) \leftrightarrow CH_4(+M)$, $C_2H_3 + H \leftrightarrow C_2H_2 + H_2$, and $H + HO_2 \leftrightarrow H_2 + O_2$ reactions are chain terminating reactions and retard flame speeds by consuming H-atoms. The flame propagation is limited by $HCO + O_2 \leftrightarrow CO + HO_2$, as this pathway is less reactive than formyl radical (HCO) decomposition. Interestingly, the laminar flame speeds exhibited a lack of sensitivity to the ethanol decomposition reactions even at fuel-rich conditions, although flame-speed sensitivity increased within the ethylene/vinyl submechanism as reflected by $C_2H_3 + H \leftrightarrow C_2H_2 + H_2$, $C_2H_2 + H(+M) \leftrightarrow C_2H_3(+M)$ and $C_2H_3 + O_2 \leftrightarrow CH_2HCO + O$. This is due to the $C_2H_5OH(+M) \leftrightarrow C_2H_4 + H_2O$ (+M) reaction.

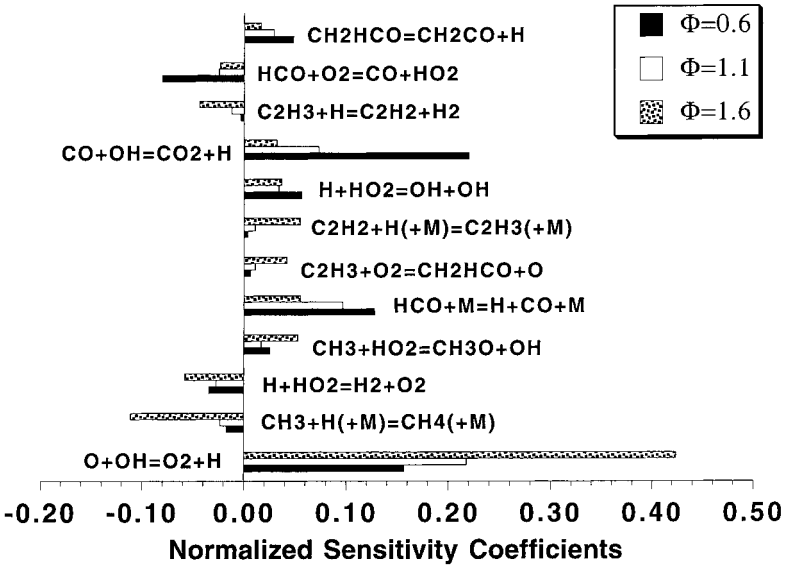

Figure 20 Normalized first order sensitivity coefficients of the most important reactions on the mass burning rate of lean, near-stoichiometric and rich ethanol/air flames at P_u = 1.0 atm and T_u = 453 K.

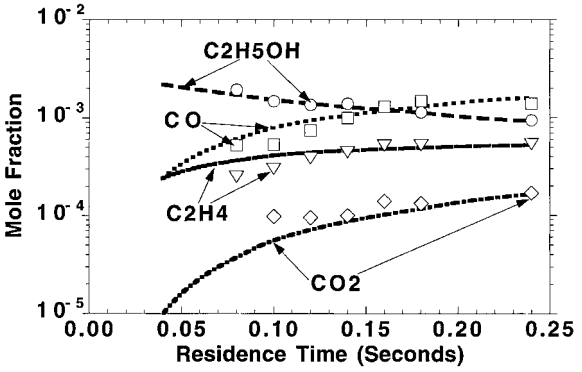

Figure 21 Ethanol—O_2—N_2 (0.3%–0.9%–98.8%) oxidation in a Jet-Stirred Reactor at $\Phi = 1.0$, 1.0 atmosphere, and a nominal temperature of 1056 K. Measurements and Predictions for C_2H_5OH, C_2H_4, CO and CO_2.

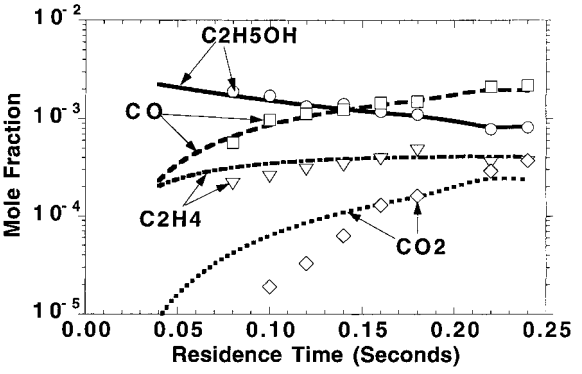

Figure 23 Ethanol—O_2—H_2 (0.3%–0.45%–99.25%) oxidation in a Jet-Stirred Reactor at $\Phi = 2.0$, 1.0 atmosphere, and a nominal temperature of 1070 K. Measurements and Predictions for C_2H_5OH, C_2H_4, CO and CO_2.

Modeling Species Concentrations from a Jet-Stirred Reactor

Aboussi [64] performed ethanol oxidation measurements in an atmospheric jet-stirred reactor. The experimental conditions covered the 1000–1200 K temperature range, and equivalence ratios of 0.2–2.0 at a fixed ethanol concentration of 0.3%. Measurements were taken as a function of residence time for CO, CO_2, CH_4, C_2H_4, C_2H_6, CH_3HCO, and C_2H_5OH. The Aboussi data set was reported later by Dagaut and coworkers in their ethanol oxidation modeling study [7]. Fair agreement was achieved between the jet-stirred reactor data and the Dagaut numerical calculations. However, their model overpredicted the ethylene and ethane concentrations, and underpredicted carbon dioxide.

The ethanol oxidation experimental data of Aboussi was used to validate the current chemical kinetic model by comparing the predicted stable species profiles to those measured in the jet-stirred reactor. The numerical computations were performed at $\phi = 1.0$ and $\phi = 2.0$, and the results are shown in Figures 21–24.

In Figure 21, a comparison of the $\phi = 1.0$ experimental data against the numerically computed species concentrations on a mole fraction basis is shown for C_2H_5OH, C_2H_4, CO, and CO_2. The modeling results show relatively good agreement with the species concentrations as the mean residence time was varied. The calculated profiles for the reaction intermediates of CH_3HCO, C_2H_6, CH_4, CH_2O, and HCOOH (Formic Acid) are shown in Figure 22. The modeling results

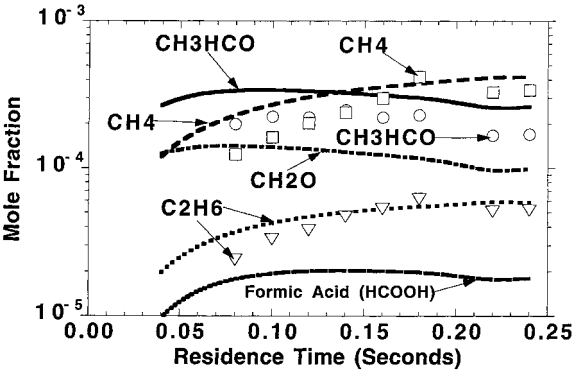

Figure 22 Ethanol—O_2—N_2 (0.3%–0.9%–98.8%) oxidation in a Jet-Stirred Reactor at $\Phi = 1.0$, 1.0 atmosphere, and a nominal temperature of 1056 K. Measurements and Predictions for CH_4, CH_3HCO, and C_2H_6. Additional Predictions shown for Formic Acid (HCOOH) and CH_2O.

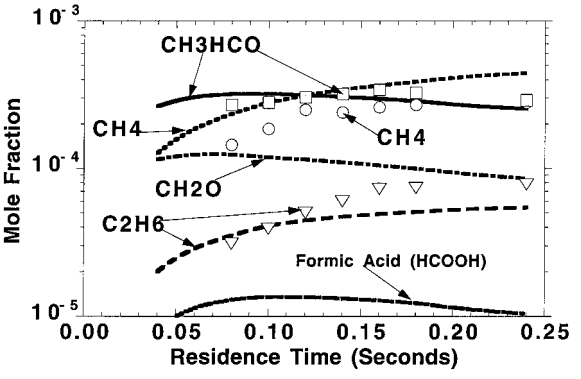

Figure 24 Ethanol—O_2—N_2 (0.3%–0.45%–99.25%) oxidation in a Jet-Stirred Reactor at $\Phi = 2.0$, 1.0 atmosphere, and a nominal temperature of 1070 K. Measurements and Predictions for CH_4, CH_3HCO, and C_2H_6. Additional Predictions shown for Formic Acid (HCOOH) and CH_2O.

show a fairly good representation of the CH_3HCO and C_2H_6 measurements. The CH_2O and HCOOH (Formic Acid) computed profiles are shown as well, although these compounds were not measured in the jet-stirred reactor study. Formaldehyde is predicted to be formed in abundance, while HCOOH is predicted in small quantities.

Reaction flux analysis was performed at $\phi = 1.0$ to determine the important ethanol consumption routes and the important production routes for the many reaction intermediates formed. Approximately 47% of the ethanol consumption flux was controlled by $C_2H_5OH + OH \leftrightarrow$ Products where $C_2H_5OH + OH \leftrightarrow CH_3CH_2O + H_2O$ was the dominating ethanol consumption reaction at 26%. The overall $C_2H_5OH + H \leftrightarrow$ Products reaction consumed 22% of the ethanol where $C_2H_5OH + H \leftrightarrow CH_3CHOH + H_2$ contributed 12% toward ethanol consumption. The $C_2H_5OH + O \leftrightarrow$ Products, $C_2H_5OH + CH_3 \leftrightarrow$ Products, and $C_2H_5OH(+M) \leftrightarrow C_2H_4 + H_2O(+M)$ reactions consumed 11%, 9%, and 8% of the ethanol, respectively. Acetaldehyde (CH_3HCO) is primarily (70%) formed through the reaction sequences of $C_2H_5OH + OH \leftrightarrow CH_3CHOH + H_2O$ (34%), and $C_2H_5OH + H \leftrightarrow CH_3CHOH + H_2$ (33%), followed by $CH_3CHOH + O_2 \leftrightarrow CH_3HCO + HO_2$, with the remainder (30%) from $C_2H_5OH + OH \leftrightarrow CH_3CH_2O + H_2O$ and $CH_3CH_2O + M \leftrightarrow CH_3HCO + H + M$. Methane formation involves several participating reactions such as $CH_3 + HO_2 \leftrightarrow CH_4 + O_2$ (27%), $CH_3 + H_2 \leftrightarrow CH_4 + H$ (14%), $CH_3HCO + CH_3 \leftrightarrow CH_3CO + CH_4$ (15%), $C_2H_5OH + CH_3 \leftrightarrow C_2H_4OH + CH_4$ (10%), and $C_2H_5OH + CH_3 \leftrightarrow CH_3CHOH + CH_4$ (19%). Ethane is formed exclusively by $CH_3 + CH_3(+M) \leftrightarrow C_2H_6(+M)$. The methyl radical is a necessary precursor species to methane and ethane formation and evolves primarily from $CH_3CH_2O + M \leftrightarrow CH_3 + CH_2O + M$ (33%), $CH_3CO(+M) \leftrightarrow CH_3 + CO(+M)$ (21%), and to a smaller extent, $CH_2HCO \leftrightarrow CH_3 + CO$ (11%), $CH_4 + OH \leftrightarrow CH_3 + H_2O$ (10%), $CH_3HCO + OH \leftrightarrow CH_3 + HCOOH$ (8%), and $CH_2CO + H \leftrightarrow CH_3 + CO$ (8%). Carbon monoxide is principally produced from $HCO + M \leftrightarrow H + CO + M$ (34%) and $HCO + O_2 \leftrightarrow CO + HO_2$ (28%), and secondarily by $CH_3CO(+M) \leftrightarrow CH_3 + CO(+M)$ (14%). Carbon dioxide production was controlled by the following reactions in order of importance: $HCCO + O_2 \leftrightarrow CO_2 + HCO$ (37%), $CO + OH \leftrightarrow CO_2 + H$ (36%), and $CO + HO_2 \leftrightarrow CO_2 + OH$ (17%). Ethylene is formed by two principal pathways. The reaction sequence of $C_2H_5OH + OH \leftrightarrow C_2H_4OH + H_2O$ and $C_2H_4OH \leftrightarrow C_2H_4OH$ contributes about 55% to ethylene production, and the remainder is due to the ethanol dehydration step, $C_2H_5OH(+M) \leftrightarrow C_2H_4 + H_2O(+M)$ (27%), and the reaction sequences $C_2H_5OH(+M) \leftrightarrow C_2H_5 + OH(+M)$ and $C_2H_5(+M) \leftrightarrow C_2H_4 + H(+M)$ (4%). Formaldehyde was predicted to be principally formed from the reaction sequence of $C_2H_5OH + OH \leftrightarrow CH_3CH_2O + H_2O$ and $CH_3CH_2O + M \leftrightarrow CH_3 + CH_2O + M$ (43%), and $CH_3 + HO_2 \leftrightarrow CH_3O + OH$ followed by $CH_3O(+M) \leftrightarrow CH_2O + H(+M)$ (34%). Formic acid (HCOOH) was predicted to be exclusively produced from acetaldehyde by the $CH_3HCO + OH \leftrightarrow CH_3 + HCOOH$ reaction.

The ethylene formation pathways deserve further comment as previous modeling studies by Norton and Dryer, and Dagaut and co-workers had easily predicted their respective ethylene profiles without the contribution from the ethanol dehydration reaction. The modeling studies from these research groups had $C_2H_5OH + OH \leftrightarrow C_2H_4OH + H_2O$ and $C_2H_4OH \leftrightarrow C_2H_4 + OH$ as the primary reaction sequence leading to ethylene production. Dagaut overpredicted the ethylene concentration while using a branching ratio value of about 0.40 at 1070 K for $k_{C_2H_5OH+OH \leftrightarrow C_2H_4OH + H_2O}/k_{C_2H_5OH+OH \leftrightarrow \text{Products}}$. Norton and Dryer used a branching value of 0.30 around 1100 K to model the ethylene concentrations seen in their turbulent flow reactor. Earlier in this study we had presented an empirical approach for predicting the branching ratio variation with temperature. A branching ratio value of approximately 0.17 was obtained around 1100 K for $k_{C_2H_5OH+OH \leftrightarrow C_2H_4OH+H_2O}/k_{\text{overall}}$ as discussed earlier. This value is lower than the values used in the previous modeling studies, and therefore the reaction sequence of $C_2H_5OH + OH \leftrightarrow C_2H_4OH + H_2O$ and $C_2H_4OH \leftrightarrow C_2H_4 + OH$ could not account for all the ethylene seen in the Aboussi experiments as well as the Norton and Dryer ethylene measurements in their turbulent flow reactor. The ethanol dehydration reaction was added to the detailed chemical kinetic model in order to overcome this problem. The combined effort of detailed chemical kinetic modeling and using RRKM/Master Equation theory for $C_2H_5OH(+M) \leftrightarrow C_2H_4 + H_2O(+M)$ and $C_2H_5OH(+M) \leftrightarrow C_2H_5 + OH(+M)$ rate constant calculations were necessary in matching the ethylene profiles shown in this study.

In Figures 23 and 24, a comparison of the $\phi = 2.0$ experimental data against the numerically computed species concentrations on a mole fraction basis is shown for C_2H_5OH, C_2H_4, CO, CO_2, CH_3HCO, C_2H_6, and CH_4. The modeling results show relatively good agreement with the species concentrations, as the mean residence time varied, although the CH_4 concentration was overpredicted. The calculated profiles for

the reaction intermediates of HCOOH, and CH_2O are also shown in Figure 24. Reaction flux analysis indicated that approximately 36% of the ethanol consumption flux is controlled by $C_2H_5OH + OH \leftrightarrow$ Products followed by $C_2H_5OH + H \leftrightarrow$ Products at 26%, $C_2H_5OH(+M) \leftrightarrow C_2H_4 + H_2O(+M)$ at 16%, and $C_2H_5OH + CH_3 \leftrightarrow$ Products at 10%. The CH_3HCO, C_2H_6, C_2H_4, CH_4, CH_2O, HCOOH, and CO reaction intermediates are produced by the same reaction sequences as discussed for the $\phi = 1.0$ case. However, the $\phi = 2.0$ case indicates that 45% of the ethylene is primarily produced by $C_2H_5OH(+M) \leftrightarrow C_2H_4 + H_2O(+M)$; the remainder is due to $C_2H_5OH + OH \leftrightarrow C_2H_4OH + H_2O$ and $C_2H_5OH + H \leftrightarrow C_2H_4OH + H_2$, followed by $C_2H_4OH \leftrightarrow C_2H_4 + OH$ at 42%; and $C_2H_5OH(+M) \leftrightarrow C_2H_5 + OH(+M)$, followed by $C_2H_5(+M) \leftrightarrow C_2H_4 + H(+M)$ at 11%.

A sensitivity analysis study was conducted for the purposes of determining the most sensitive reactions that strongly influence the overall rate of ethanol oxidation at stoichiometric and rich conditions. Figures 25 and 26 show the normalized sensitivity coefficients important to ethanol consumption for the $\phi = 1.0$ and $\phi = 2.0$ cases. If the sensitivity coefficient exhibits a positive value or ($\downarrow$), that would indicate a decrease in the overall reactivity of the ethanol oxidation system, and a negative value or ($\uparrow$) would imply an increase in the overall reactivity of the ethanol oxidation system. For the conditions found in the Aboussi experiments, the six most sensitive reactions to the overall rate of ethanol oxidation at stoichiometric and rich conditions, in order of their peak sensitivity coefficients, are

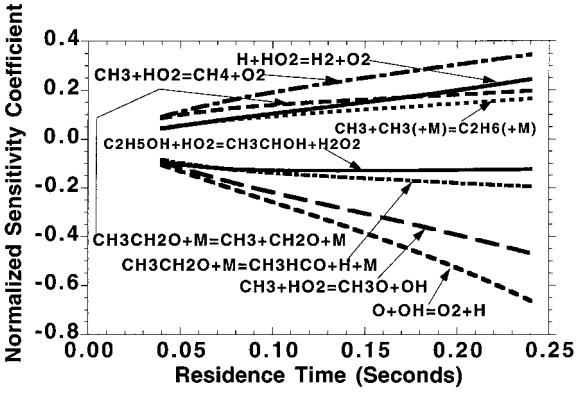

Figure 25 Sensitivity Results for Ethanol—O_2—N_2 oxidation in a Jet-Stirred Reactor for $\Phi = 1.0$ case.

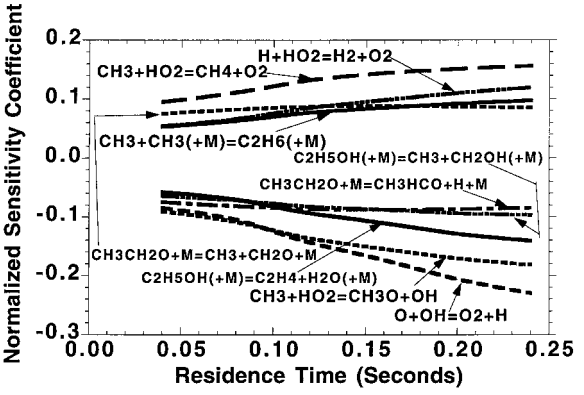

Figure 26 Sensitivity Results for Ethanol—O_2—N_2 oxidation in a Jet-Stirred Reactor for $\Phi = 2.0$ case.

$$(\uparrow)\ H + O_2 \longleftrightarrow OH + O \quad (-2)$$

$$(\uparrow)\ CH_3 + HO_2 \longleftrightarrow CH_3O + OH \quad (27)$$

$$(\downarrow)\ CH_3 + HO_2 \longleftrightarrow CH_4 + O_2 \quad (28)$$

$$(\downarrow)\ CH_3CH_2O + M \longleftrightarrow CH_3 + CH_2O + M \quad (150)$$

$$(\downarrow)\ H + HO_2 \longleftrightarrow H_2 + O_2 \quad (7)$$

$$(\uparrow)\ CH_3CH_2O + M \longleftrightarrow CH_3CHO + H + M \quad (149)$$

The $H + O_2 \leftrightarrow OH + O$ chain branching reaction exhibits a large negative sensitivity coefficient that increases with mean residence time. This is caused by additional fuel consumption which allows for greater H-atom generation at longer residence times. The H-atom sources are $HCO + M \leftrightarrow H + CO + M$, $CH_3CH_2O + M \leftrightarrow CH_3HCO + H + M$, $CH_2HCO + M \leftrightarrow CH_2CO + H + M$, $CH_3O + M \leftrightarrow CH_2O + H + M$, and $OH + H_2 \leftrightarrow H_2O + H$.

The CH_3CH_2O decomposition reactions exhibited a large positive and negative sensitivity coefficient, as shown in Figures 25 and 26. The branching ratio for CH_3CH_2O decomposition to $CH_3HCO + H$ and $CH_3 + CH_2O$ products was largely determined by matching the measured CH_3HCO, CH_4, and C_2H_5OH profiles in the jet-stirred and turbulent flow reactor modeling study. The rate constant assigned to each reaction was verified by performing a QRRK analysis on the $CH_3 + CH_2O \leftrightarrow CH_3CH_2O \leftrightarrow CH_3HCO + H$ reaction network, and the results are shown for 1.0 atm in Table I. Interestingly, reaction flux analysis indicates $C_2H_5OH + OH \leftrightarrow CH_3CH_2O + H_2O$ as one of the most important ethanol consuming reactions yet this reaction does not appear as a very sensitive reaction to the overall ethanol oxidation rate. This finding is a little misleading in that the sensitivity exhibited by

$C_2H_5OH + OH \leftrightarrow$ Products is largely due to the radical it produces. In the case of $C_2H_5OH + OH \leftrightarrow CH_3CH_2O + H_2O$, the CH_3CH_2O radical decomposes to either $CH_3HCO + H$ or $CH_3 + CH_2O$ products. Each pathway negates the other on their respective affect on the overall ethanol oxidation rate. This would explain why the $C_2H_5OH + OH \leftrightarrow CH_3CH_2O + H_2O$ reaction does not appear to be sensitive. It must be emphasized that the branching ratios selected for $C_2H_5OH + OH \leftrightarrow$ Products are important in determining the correct product profiles found in the ethanol oxidation jet-stirred and flow reactor studies as well as obtaining the correct overall reactivity exhibited within the chemical system.

The sensitivity analysis results also show the important influence the HO_2 radical has on the overall ethanol oxidation rate. Chain terminating reactions like $CH_3 + HO_2 \leftrightarrow CH_4 + O_2$ and $H + HO_2 \leftrightarrow H_2 + O_2$ tend to retard the ethanol oxidation process as they limit radical pool growth. Chain propagating reactions like $CH_3 + HO_2 \leftrightarrow CH_3O + OH$ (followed by $CH_3O + M \leftrightarrow CH_2O + H + M$) and $H + HO_2 \leftrightarrow OH + OH$ tend to increase the rate of ethanol oxidation as these reactions convert the unreactive HO_2 radical to a reactive OH radical. The $C_2H_5OH + HO_2 \leftrightarrow CH_3CHOH + H_2O_2$ reaction is shown to be a sensitive reaction at short mean residence times, although reaction flux analysis indicates that this reaction contributes no more than 2.0% of the ethanol consumption flux. The limited amount of ethanol conversion at the short residence times favors HO_2 production and the chain branching that occurs through H_2O_2 decomposition. This is explained by the reaction sequence of $C_2H_5OH + HO_2 \leftrightarrow CH_3CHOH + H_2O_2$, $CH_3CHOH + O_2 \leftrightarrow CH_3HCO + HO_2$ followed by $H_2O_2 + M \leftrightarrow OH + OH + M$.

The $C_2H_5OH(+M) \leftrightarrow C_2H_4 + H_2O(+M)$ reaction exhibits greater sensitivity with increasing equivalence ratio and is shown to be a very sensitive reaction at $\phi = 2.0$. Reaction flux analysis shows the ethanol dehydration process commands a greater fraction of the ethanol consumption flux at progressively rich conditions. This finding supports the sensitivity analysis results.

Modeling Species Concentrations from a Flow Reactor

Norton and Dryer [6,13] performed an experimental and modeling study of ethanol oxidation kinetics in a turbulent flow reactor. They reported experimental profiles of the stable species concentrations and temperatures for ethanol oxidation at atmospheric pressure, initial temperatures near 1100 K, and the equivalence ratio range of 0.61–1.24. They found acetaldehyde, ethylene and methane in nearly equal concentrations as the major reaction intermediates produced for the experimental conditions examined. Their chemical kinetic modeling results showed very good agreement with the experimental data, and they noted the importance of selecting the proper branching ratios for reactions involving ethanol with OH and H-atom.

The experimental data of Norton and Dryer were used to validate the current chemical kinetic model by comparing the predicted stable species profiles to those measured during the ethanol oxidation process. The numerical computations were performed at $\phi = 0.61$ and $\phi = 1.24$, and the results are shown in Figures 27–31.

In Figures 27 and 28, a comparison of the experimental data against the numerically computed species concentrations on a mole percent basis is shown for C_2H_5OH, O_2, CO, CO_2, H_2, and H_2O. Due to the uncertainty in the experimental induction time, the numerical results had to be "time shifted" [6] to match the experimental data at the 50% fuel decay point. The amount of the shift was approximately 24 milliseconds for $\phi = 0.61$ and 23 milliseconds for $\phi = 1.24$. The results show relatively good agreement. The model was unable to reproduce the ethanol consumption profile for the $\phi = 0.61$ case. The difference in the initial slope of the ethanol profile may be due to the reported uncertainty in the measured temperature profile that

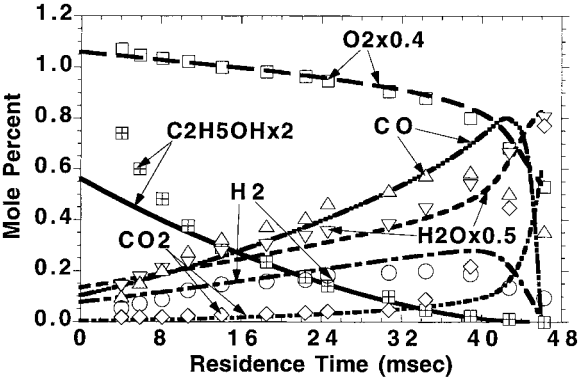

Figure 27 Comparison between experimental (symbols) flow reactor oxidation data for $\phi = 0.61$ as investigated by Norton and Dryer [6] and the numerical calculations (lines) using the detailed chemical kinetic model. The numerical results were time "shifted" by ca. −24 msec. Experimental conditions: 5.65% C_2H_5OH, 2.786% O_2, and 96.649% Nitrogen, Reynolds Number = 7140, P = 1 atm., and T_{in} = 1092 K. Numerical simulations shown for C_2H_5OH, O_2, CO, CO_2, H_2, and H_2O.

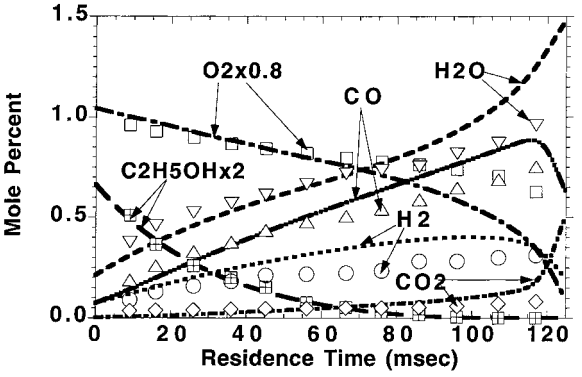

Figure 28 Comparison between experimental (symbols) flow reactor oxidation data for $\phi = 1.24$ as investigated by Norton and Dryer [6] and the numerical calculations (lines) using the detailed chemical kinetic model. The numerical results were time "shifted" by ca.−23 msec. Experimental conditions: 5.81% C_2H_5OH, 1.407% O_2, and 98.012% Nitrogen, Reynolds Number = 4900, P = 1atm, and T_{in} = 1100 K. Numerical simulations shown for C_2H_5OH, O_2, CO, CO_2, H_2, and H_2O.

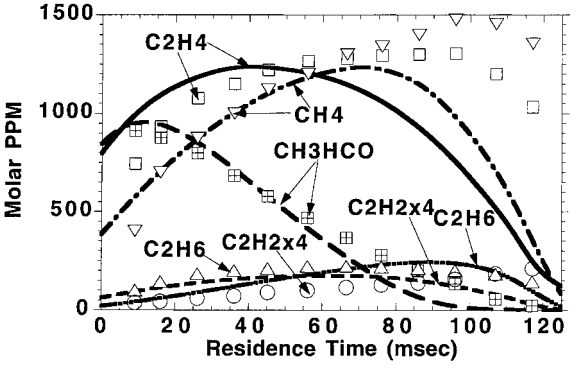

Figure 30 Comparison between experimental (symbols) flow reactor oxidation data for $\phi = 1.24$ as investigated by Norton and Dryer [6] and the numerical calculations (lines) using the detailed chemical kinetic model. The numerical results were time "shifted" by ca. −23 msec. Experimental conditions: 5.81% C_2H_5OH, 1.407% O_2, and 98.012% Nitrogen, Reynolds Number = 4900, P = 1 atm, and T_{in} = 1100 K. Numerical simulations shown for CH_3HCO, C_2H_4, CH_4, C_2H_6, and C_2H_2.

was estimated to be ±10 K. The O_2, H_2, H_2O, and CO_2 species were shown to be fairly well predicted, and the CO profile was reasonably predicted. The calculated profiles for the reaction intermediates, CH_4, C_2H_2, C_2H_4, C_2H_6, CH_3HCO, and C_3H_6 are shown in Figures 29–31. The numerical results show a fair representation of the CH_3HCO, C_2H_6, C_2H_4, C_2H_2, and C_3H_6 profiles, although additional modeling effort would ultimately yield better agreement than shown in the figures.

Reaction flux analysis was performed to determine the important ethanol consumption and production routes for the many reaction intermediates formed. Ethanol is primarily consumed by $C_2H_5OH + OH \leftrightarrow$ Products and secondarily by $C_2H_5OH + O \leftrightarrow$ Products and $C_2H_5OH + H \leftrightarrow$ Products at the lean conditions of the turbulent flow reactor. Acetaldehyde was primarily produced through the reaction sequence

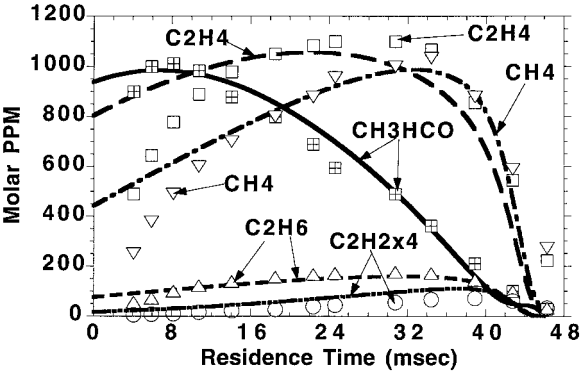

Figure 29 Comparison between experimental (symbols) flow reactor oxidation data for $\phi = 0.61$ as investigated by Norton and Dryer [6] and the numerical calculations (lines) using the detailed chemical kinetic model. The numerical results were time "shifted" by ca. −24 msec. Experimental conditions: 5.65% C_2H_5OH, 2.78% O_2, and 96.649% Nitrogen, Reynolds Number = 7140, P = 1 atm, and T_{in} = 1092 K. Numerical simulations shown for CH_3HCO, C_2H_4, CH_4, C_2H_6, and C_2H_2.

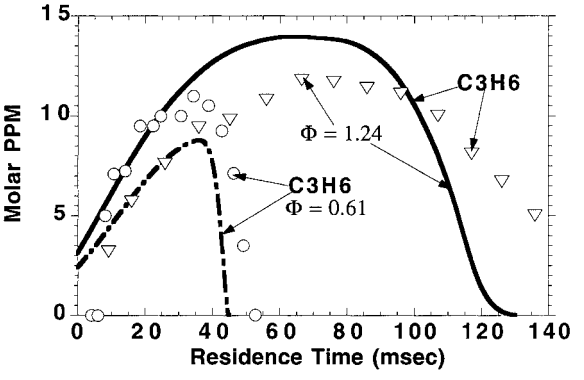

Figure 31 Comparison between experimental (symbols) flow reactor oxidation data for $\phi = 0.61$ and $\phi = 1.24$ as investigated by Norton and Dryer [6] and the numerical calculations (lines) using the detailed chemical kinetic model. Numerical simulation shown for C_3H_6 (propene).

of $C_2H_5OH + OH \leftrightarrow CH_3CHOH + H_2O$ followed by $CH_3CHOH + O_2 \leftrightarrow CH_3HCO + HO_2$, and secondarily by $C_2H_5OH + OH \leftrightarrow CH_3CH_2O + H_2O$ and $CH_3CH_2O + M \leftrightarrow CH_3HCO + H + M$. Methane formation is primarily controlled by $CH_3 + HO_2 \leftrightarrow CH_4 + O_2$, $C_2H_5OH + CH_3 \leftrightarrow CH_3CHOH + CH_4$, and $CH_3HCO + CH_3 \leftrightarrow CH_3CO + CH_4$. Ethane was formed exclusively by $CH_3 + CH_3 (+M) \leftrightarrow C_2H_6(+M)$. Ethylene was produced by the reaction sequence of $C_2H_5OH + OH \leftrightarrow C_2H_4OH + H_2O$ and $C_2H_5OH + H \leftrightarrow C_2H_4OH + H_2$ followed by $C_2H_4OH \leftrightarrow C_2H_4 + OH$, ethanol dehydration, and $C_2H_5OH(+M) \leftrightarrow C_2H_5 + OH(+M)$ followed by $C_2H_5(+M) \leftrightarrow C_2H_4 + H(+M)$. Acetylene was produced by way of the ethylene intermediate compound. The reaction sequence of $C_2H_4 + OH \leftrightarrow C_2H_3 + H_2O$, $C_2H_3 + O_2$ metathesis to $C_2H_2 + HO_2$, and $C_2H_3(+M) \leftrightarrow C_2H_2 + H(+M)$ contributed to the acetylene formation as measured in the experiment. Lastly, propene (C_3H_6) was formed by the vinyl (C_2H_3) and methyl (CH_3) radical combination reaction.

A sensitivity analysis study was conducted for the purpose of determining the most sensitive reactions that strongly influence the overall rate of ethanol oxidation. The analysis was performed by perturbing the forward and reverse rate constants for each reaction by a factor of two, thereby leaving the thermochemistry or thermodynamic equilibrium constant within the chemical reaction unaffected. The sensitivity coefficient was then determined by taking the natural logarithm of the mole fraction of ethanol remaining after 25 milliseconds of computed oxidation time with the perturbed reaction kinetics divided by the baseline mole fraction of ethanol. The sensitivity coefficient is expressed as $S = -\ln(X_{C_2H_5OH,pert} X_{C_2H_5OH,unpert})$. If the sensitivity coefficient exhibits a negative value that would indicate a decrease in the overall reactivity of the chemical system, and a positive value would imply an increase in the overall reactivity of the chemical system. Figure 32 shows the results of the sensitivity analysis performed for the $\phi = 0.61$ case. The $H + O_2 \leftrightarrow OH + O$ reaction is shown to be the most sensitive reaction to the overall rate of ethanol oxidation at lean conditions, followed by $CH_3 + HO_2 \leftrightarrow CH_3O + OH$, $CH_3 + HO_2 \leftrightarrow CH_4 + O_2$, CH_3CH_2O decomposition to $CH_3 + CH_2O$ and $CH_3HCO + H$, $C_2H_5OH + HO_2 \leftrightarrow CH_3CHOH + H_2O_2$, and $C_2H_5OH(+M) \leftrightarrow CH_3 + CH_2OH(+M)$. The $H + O_2 \leftrightarrow OH + O$ chain branching reaction affects the OH and O-atom radical pool, as noted by the large positive sensitivity coefficient. These reactive radicals are important to consuming ethanol. The $CH_3 + HO_2 \leftrightarrow CH_3O + OH$ reaction enhances the ethanol oxidation rate and this is largely due to the conversion of two unreactive radicals (i.e., CH_3, HO_2) to two reactive radicals (i.e., OH, H) through the reaction sequence of $CH_3 + HO_2 \leftrightarrow CH_3O + OH$ followed by $CH_3O(+M) \leftrightarrow CH_2O + H(+M)$. The $CH_3 + HO_2 \leftrightarrow CH_4 + O_2$ shows a negative sensitivity coefficient due to the chain terminating nature of the reaction. The $CH_3CH_2O + M \leftrightarrow CH_3 + CH_2O + M$ and $CH_3CH_2O + M \leftrightarrow CH_3HCO + H + M$ decomposition reactions exhibit opposing sensitivity coefficient values. This result shows the role H-atom and CH_3 radicals play in increasing or decreasing the eth-

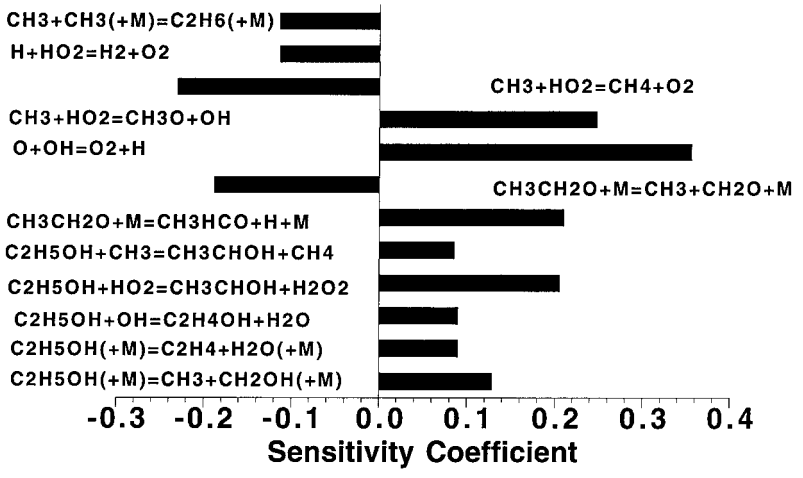

Figure 32 First order sensitivity coefficients of the important reactions affecting the ethanol consumption rate. See text for discussion. Experimental conditions: 5.65% C_2H_5OH, 2.786% O_2, and 96.649% Nitrogen, Reynolds Number = 7140, P = 1atm, and T_{in} = 1092 K.

anol consumption rate by its impact on the radical pool. The $C_2H_5OH + HO_2 \leftrightarrow CH_3CHOH + H_2O_2$ reaction has a fairly large positive sensitivity coefficient at lean conditions as the conversion of HO_2 to H_2O_2 can lead to OH radical production by $H_2O_2 (+M) \leftrightarrow OH + OH(+M)$. However, $C_2H_5OH + HO_2 \leftrightarrow CH_3CHOH + H_2O_2$ does not contribute significantly to the ethanol consumption flux in spite of the sensitivity analysis results. The $C_2H_5OH + OH \leftrightarrow$ Products reactions exhibit small sensitivity coefficients, although ethanol consumption by OH radicals is very important to ethanol oxidation. The positive sensitivity coefficients shown for $C_2H_5OH (+M) \leftrightarrow C_2H_4 + H_2O(+M)$ and $C_2H_5OH(+M) \leftrightarrow CH_3 + CH_2OH(+M)$ reflect the importance of ethanol decomposition at these conditions.

SUMMARY

A chemical kinetic modeling investigation was presented which successfully reproduced the measurements from five different experimental systems. The modeling study of ignition delay in shock tubes noted the importance of the $C_2H_5OH(+M) \leftrightarrow CH_3 + CH_2OH(+M)$, $C_2H_5OH(+M) \leftrightarrow C_2H_5 + OH(+M)$ and $O + OH \leftrightarrow O_2 + H$ reactions. Ignition delay times were successfully reproduced when representing the ethanol decomposition reactions as pseudo-first order rate expressions using the Troe format for fall-off kinetics. The modeling study of laminar flame speeds in freely propagating flames showed that proper characterization of the H-atom production and consumption steps, and HCO and CO oxidation kinetics are very important for proper ethanol-air flame speed prediction. Jet-stirred and turbulent flow reactor modeling of ethanol oxidation showed the importance of the $C_2H_5OH + OH \leftrightarrow$ Products reaction and its branching ratio selection, and the reaction kinetics for $C_2H_5OH(+M) \leftrightarrow C_2H_4 + H_2O(+M)$ over a wide range of equivalence ratios. Sensitivity analysis showed at all equivalence ratios the relative importance of the $H + O_2$ chain branching reaction; $C_2H_5OH + OH \leftrightarrow$ Products; CH_3CH_2O decomposition to $CH_3 + CH_2O$ and $CH_3HCO + H$ products; and HO_2 reactions with CH_3, H-atom, and ethanol. Lastly, an empirical procedure was used to derive the branching ratios for $C_2H_5OH + OH$, $C_2H_5OH + O$, $C_2H_5OH + H$, and $C_2H_5OH + CH_3$ reactions that was instrumental to the success of the high temperature ethanol oxidation model validation study.

The modeling work was performed under the auspices of the U.S. Department of Energy by the Lawrence Livermore National Laboratory under contract No. W-7405-ENG-48.

BIBLIOGRAPHY

1. Carlsen, W. San Francisco Chronicle; September 15, 1997.
2. Natarajan K.; Bhaskaran, K. A. Thirteenth International Shock Tube Symposium; Niagara Falls, 1981; p 834.
3. Dunphy, M. P.; Simmie, J. M. J Chem Soc Faraday Trans 1991, 87, 1691–1695, 2549–2559.
4. Egolfopolous, F. N.; Du, D. X.; Law, C. K. Twenty-Fourth Symposium (International) on Combustion; The Combustion Institute, 1992; p 833.
5. Borisov, A. A.; Zamanskii, V. M.; Konnov, A. A.; Lisyanskii, V. V.; Rusakov, S. A.; Skachov, G. I. Soviet J Chemical Physics 1991, 8, 121–141; and 1992, 9, 2527–2537.
6. Norton, T. S.; Dryer, F. L. Int J Chem Kinet 1992, 24, 319–344.
7. Dagaut, P.; Cathonnet, M.; Boettner, J. C. J Chim Phys 1992, 89, 867–884.
8. Cullis, C. F.; Newitt, E. J. Proc Royal Soc London 1956, 237A, 530; and 1956, 242A, 516.
9. Freeman, G. R. Proc Royal Soc London 1958, 245A, 75.
10. Barnard, J. A.; Hughes, H. W. D. Trans Faraday Soc 1960, 56, 55.
11. Brown, J.; Tipper, C. F. H. Proc Royal Soc London 1969, 312A, 399.
12. Rotzoll, G. J Anal Appl Pyrol 1985, 9, 43.
13. Norton, T. S.; Dryer, F. L. Twenty-Third Symposium (International) on Combustion; The Combustion Institute, 1990; pp 179–185.
14. Taylor, P. H.; Shanbhag, S.; Dellinger, B. Society of Automotive Engineers 1994, 941904.
15. Lee, D.; Hochgreb, S.; Keck, J. C. Society of Automotive Engineers 1993, 932755.
16. Naegeli, D. W.; Weatherford, W. D. Jr. Fuel 1989, 68, 45–48.
17. Gulder, O. L. Nineteenth Symposium (International) on Combustion; The Combustion Institute, 1982; p 275.
18. Smith, S. R.; Gordon, A. S. J Phys Chem 1956, 60, 1059.
19. Lieb, D. F.; Roblee, L. H. S. Jr. Combust Flame 1970, 14, 285–296.
20. Curran, H. J.; Dunphy, M. P.; Simmie, J. M.; Westbrook, C. K.; Pitz, W. J. Twenty-Fourth Symposium (International) on Combustion; The Combustion Institute, 1992; p 769; also Curran, H. J. personal communication, 1997.
21. Kee, R. J.; Rupley, F. M.; Miller, J. A. "CHEMKIN-II: A Fortran Chemical Kinetics Package for the Analysis of Gas Phase Chemical Kinetics"; Sandia Report #SAND 89-8009; Sandia National Laboratories, 1989.

22. Lutz, A. E.; Kee, R. J.; Miller, J. A. "SENKIN: A Fortran Program for Predicting Homogeneous Gas Phase Chemical Kinetics with Sensitivity Analysis"; Sandia Report #SAND87-8248; Sandia National Laboratories, 1987.
23. Kee, R. J.; Grcar, J. F.; Smooke, M. D.; Miller, J. A. "A Fortran Program for Modelling Steady One-Dimensional Premixed Flames"; Sandia Report #SAND85-8420; Sandia National Laboratories, 1985.
24. Galrborg, P.; Kee, R. J.; Grcar, J. F.; Miler, J. A. "PSR: A Fortran program for Modelin Well-Stirred Reactors"; Sandia Report #86-8209: Sandia National Laboratories, 1986.
25. Marinov, N. M.; Westbrook, C. K.; Pitz, W. J. Transport Phenomena in Combustion; Chen, S. H., Ed.; Eighth International Symposium on Transport Processes; 1996; p 118.
26. Marinov, N. M.; Pitz, W. J.; Westbrook, C. K.; Castaldi, M. J.; Senkan, S. M. Comb Sci and Tech 196, 116–117, 211–287.
27. Castaldi, M. J.; Marinov, N. M.; Melius, C. F.; Huang, J.; Senkan, S. M.; Pitz, W. J.; Westbrook, C. K. Twenty-Sixth Symposium (International) on Combustion; The Combustion Institute, 1996; pp 693–702.
28. Marinov, N. M.; Malte, P. C. Int J Chem Kinet 1995, 27, 957.
29. Marinov, N. M.; Castaldi, M. J.; Melius, C. F.; Tsang, W. Combust Sci and Tech 1997, 128, 295–342.
30. Kee, R. J.; Dixon-Lewis, G.; Warnatz, J.; Coltrin, M. E.; Miller, J. A. "The Chemkin Transport Database"; Sandia Report #SAND86-8246; Sandia National laboratories, 1986.
31. Wang, H.; Frenklach, M. Combust Flame 1994, 96, 163.
32. Kee, R. J.; Rupley, F. M.; Miller, J. A. "The Chemkin Thermodynamic Database"; Sandia Report #SAND87-8215B; Sandia National Laboratories, 1987.
33. Burcat, A.; McBride, B. "1994 Ideal Gas Thermodynamic Data for Combustion and Air-Pollution Use"; Technion Report #TAE 697, 1993.
34. Benson, S. W. Thermochemical Kinetics, 2nd Ed.; John Wiley & Sons: New York, 1976.
35. Cohen, N.; Benson, S. W. Chem Rev 1993, 93, 2419.
36. Ritter, E. R.; Bozzelli, J. W. Int J Chem Kinet 1991, 23, 767–778.
37. Gordon, S.; McBride, B. J. "Computer Program for Calculation of Complex Chemical Equilibrium Compositions, Rocket Performance, Incident and Reflected Shocks and Chapman-Jouget Detonations"; NASA SP-273, 1971.
38. Meier, U.; Grotheer, H. H.; Riekert, G.; Just, Th. Ber Bunsenges Physik Chem 1985, 89, 325.
39. Hess, W. P.; Tully, F. P. Chem Phys Lett 1989, 152, 183–189.
40. Washida, N. J Chem Phys 1981, 75, 2715.
41. Dutton, N. J.; Fletcher, I. W.; Whitehead, J. C. J Phys Chem 1985, 89, 569–570.
42. Gray, P.; Herod, A. A. Trans Faraday Soc 1968, 64, 1568–1576.
43. Bott, J. F.; Cohen, N. Int J Chem Kinet 1991, 23, 1075–1094.
44. Tsang, W. J Phys Chem Ref Data 1987, 16, 471.
45. Cohen, N. Int J Chem Kinet 1991, 23, 683–691.
46. Avramenko, L. I.; Kolesnikova, R. V. Bull Acad Sci USSR Div Chem Sci 1971, 20, 2700.
47. Dzotsenidze, Z. G.; Oganesyan, K. T.; Sachyan, G. A.; Nalbandyan, A. Arm Khim Zh 1967, 20, 983.
48. Tsang, W. J Phys Chem Ref Data 1988, 17, 887.
49. Tsang, W. J Phys Chem Ref Data 1990, 19, 1–68.
50. Gilbert, R. G.; Smith, S. C.; Jordan, M. J. T. UNIMOL Program Suite, 1993.
51. Smith, G. P.; Golden, D. M. Int J Chem Kinet 1978, 10, 489–501.
52. Green, J. H. S. Trans Faraday Soc 1961, 57, 2132–2137.
53. Chase, M. W. Jr.; Davies, C. A.; Downey, J. R. Jr.; Frurip, D. J.; McDonald, R. A.; Syverud, A. N. J Phys Chem Ref Data 1985, 14, Suppl. No. 1, JANAF Tables.
54. Stewart, J. J. P. MOPAC 93.00 Manual; Fujitsu Limited: Tokyo, 1993.
55. Seetula, J. A.; Gutman, D. J Phys Chem 1992, 96, 5401.
56. Herzler; J.; Manion, J. A.; Tsang, W. J. Phys Chem A 1997, 101, 5494–5499, 5500–5508.
57. Butkovskaya, N. I.; Zhao, Y.; Setser, D. W. J Phys Chem 1994, 98, 10779–10786.
58. Butkovskaya, N. I.; Setser, D. W. J Chem Phys 1996, 105, 8064–8074.
59. Walch, S. P. J Chem Phys 1993, 98, 3163–3167.
60. Zhitneva, G. N.; Pshezhetskii, S. Kh Vys Energ 1985, 19, 176–181; and 1986, 20, 477–479.
61. Lewis, D.; Keil, M. Sarr, M. J Am Chem Soc 1974, 96, 4390.
62. Tsang, W. Int J Chem Kinet 1976, 8, 193–203.
63. Cooke, D. F.; Dodson, M. G.; Williams, A. Combust Flame 1971, 16, 233.
64. Aboussi, B. Ph.D. Dissertation, Orleans, 1991.
65. Tsang, W. J Phys Chem Ref Data 1986, 15, 1087.
66. Avillez Pereira, R. De; Baulch, D. L.; Pilling, M. J.; Robertson, S. H.; Zeng, G. J Phys Chem A 1997, 101, 9681–9693.
67. Bowman, C. T.; Hanson, R. K.; Davidson, D. F.; Gardiner, W. C. Jr.; Lissianski, V.; Smith, G. P.; Golden, D. M.; Frenklach, M. Goldenberg, M. http://www.me.berkeley.edu/gri_mech/1997.
68. Dean, A. M.; Bozzelli, J. W. In Combustion Chemistry II; Gardiner, W. C. Jr., Ed.; Springer-Verlag: New York, 1997.
69. Saito, K.; Kakumoto, T.; Kuroda, N.; Torii, S.; Imamura, A. J Chem Phys 1984, 80, 4989.
70. Hartmann, D.; Karthauser, J.; Sawerysyn, J. P.; Zellner, R. Ber Bunsenges Phys Chem 1990, 94, 639.
71. Taylor, P. H.; Rahman, M. S.; Arif, M.; Dellinger, B.; Marshall, P. Twenty-Sixth Symposium (International) on Combustion; The Combustion Institute, 1996; pp 497–504.
72. Pitz, W. J., personal communication, 1997.

73. Atkinson, R. Chem Rev 1986, 86, 69.
74. Lodhi, Z. H.; Walker, R. W. J Chem Soc Faraday Trans 1991, 87, 681–689.
75. Pauwels, J. F.; Volponi, J. V.; Miller, J. A. Combust Sci and Tech 1995, 111, 249–276.
76. Melius, C. F., personal communication, 1997.
77. Aders, W. K.; Wagner, H. Gg. Ber Bunsenges Phys Chem 1973, 77, 712.
78. Grotheer, H. H.; Nesbitt, F. L.; Klemm, R. B. J Phys Chem 1986, 90, 2512; BNL Informal Report No. 37971, 1986.
79. Baulch, D. L.; Cobos, C. J.; Cox, R. A.; Esser, C.; Frank, P.; Just, Th.; Kerr, J. A.; Pilling, M. J.; Troe, J.; Walker, R. W.; Warnatz, J. J Phys Chem Ref Data 1992, 21, 411–429.
80. Reid, R. C.; Prausnitz, J. M.; Poling, B. E. The Properties of Gases and Liquids; McGraw-Hill, Inc., 1987.
81. Miller, J. A., personal communication, 1994.
82. Held, T. J.; Dryer, F. L., Int J Chem Kinet 1998, 30, 805–830.